

1

Electronic excitations in solar cells from *GW* approaches

Silvana Botti and Julien Vidal

Laboratoire des Solides Irradiés and ETSF, École Polytechnique, CNRS, CEA-DSM, 91128 Palaiseau, France
Université de Lyon and LPMC, CNRS, UMR 5586, Université Lyon 1, F-69622 Villeurbanne, France

1.1 Thin-film photovoltaics

The energy received by the Earth from the Sun (with a rate of 174 PW in the upper atmosphere) is by far larger than the current world energy consumption. In view of the present crisis of the dominant energy resources and the raising concern about environment, solar power emerges as a concrete alternative for a sustainable and environment friendly growth of the world energy supply (Green 2000).

The discovery of the photovoltaic (PV) effect by Alexandre Edmond Becquerel in 1839 provided a way to convert directly solar radiation into electricity. Despite the fact that the thermodynamic limit for the efficiency of a PV device is about 85.0%, according to the Carnot law, the first solar cells, made of gold coated selenium, were only around 1% efficient. The first modern PV cells, with an energy conversion efficiency of about 6%, were built only in the 50s at Bell laboratories by Chapin et al. (2004) using silicon. Chapin and coworkers invented the basic design for solar devices that would be used in the following 60 years. At the heart of the cell there is the p-n junction, obtained by placing in contact a p-doped and a n-doped semiconductor. When two materials with opposite type of doping are put together, an electric field is built at the interface, in the so-called space-charge region. This electric field drives the separation of the positively charged hole and the negatively charged electron that are

generated when a photon is absorbed. The charges further diffuse to the electrodes through the so-called quasi-neutral region and finally create a current by recombining in the external circuit. (Sze and Ng 2007)

The PV technology of the first generation relied almost exclusively on one material: silicon. Indeed, silicon was the only semiconductor whose growth was mastered to the extent required for the precise control of doping and impurity concentration (Pearson 1957). Since the 50s, the increasing performance of crystalline silicon solar cells has benefited from the technological progresses in semiconductor industry. Despite reaching record efficiencies of 25% (Zhao et al. 1998) and despite its domination on the solar cell market, the PV technology based on crystalline silicon struggles to break the symbolic 1\$/W barrier. The reduction of costs is mainly limited by the requirement of growing a thick layer of highly pure silicon. In fact, due to the indirect gap of silicon and the consequent poor absorption of light at the onset, a crystalline layer of 100 μm is necessary in order to generate enough electron-hole pairs. Moreover, a high purity is required to increase the diffusion length of electrons and holes in the quasi-neutral region, in order to assure that the charges reach the electrical contacts before recombining. For years this issue has impaired seriously the viability of photovoltaic solar power, making it hard to compete with traditional energy resources (Wadia et al. 2009).

A second generation technology based on thin-film absorbers emerged already 30 years ago, with the main goal of decreasing the production costs of solar panels (Shah et al. 1999). At the heart of the device there is still a p-n junction that is responsible for the separation of charge carriers. In contrast with crystalline absorbing layers of hundreds of μm , thin-film absorbers are just 2–3 μm thick. The thickness of the absorber layer can be reduced only if extremely efficient light-harvesting materials are employed: that is why materials such as CdTe (Wu et al. 2001) and Cu(In,Ga)(Se,S)₂ (Jackson et al. 2011), with remarkably large absorption coefficients, are ideal absorbers in thin-film photovoltaics. The use of thin-films implies significant saving on the quantity of material required. Besides, it brings a simplification in the growth processes and allows for the introduction of new substrates. Thanks to that, the 1\$/W barrier becomes accessible even if thin-film solar cells still display lower conversion efficiencies than their crystalline silicon counterparts.

In comparison to the first solar cells produced in the 50s, the design of thin-film devices underwent some essential changes. Figure 1.1 displays the scheme of a thin-film solar cell: at least four different materials with specific electrical and optical properties are stacked. The single material properties that determine the PV efficiency, and that one would like to control, are band gaps, doping levels, and absorption coefficients. In addition, also band offsets at the interfaces, which depend on the structure of the interface, on doping levels, and on band-edge alignments, have a strong influence on the device performance. These electronic properties are nowadays getting accessible and predictable via *ab initio* calculations.

In this chapter we present the state-of-the-art *ab initio* approaches able to determine electronic states and optical properties of complex compounds used

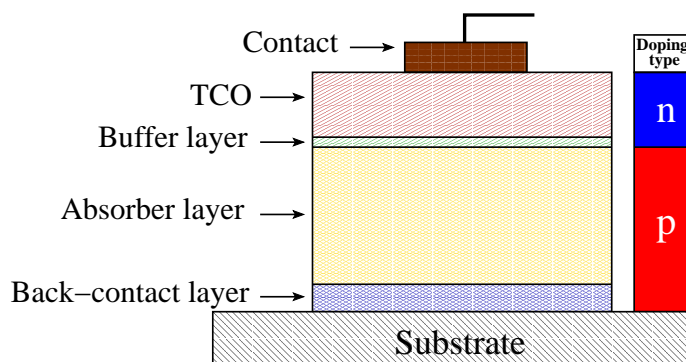


Figure 1.1 Schematic description of a thin-film solar cell. TCO stands for transparent conducting oxide.

in thin-film solar cells. Such approaches are based on the GW approximation within many-body perturbation theory. This is a rapidly expanding field of investigation and it is not possible to include here all recent developments. We decided therefore to focus on two applications, Cu-based absorbers and Cu-based transparent conducting oxides, and to use these examples to discuss achievements and limitations of the most accurate theories.

For the past years, there has been a substantial effort to study the properties of Cu-based compounds for photovoltaics, not only to understand them from a fundamental point of view, but also to optimize their properties and design solar cells with better performance. However, there is still a clear lack of consistent theoretical and computational studies that can explain and describe electronic excitations in this class of materials. As a consequence, whenever silicon is not used as an absorber, a major obstacle for a fast development of highly efficient devices is the lack of knowledge of basic material properties, in particular related to defect physics. In fact, silicon and other III-V semiconductors have also a broad use outside the world photovoltaics, e.g. in electronics, lasers, LEDs, and therefore a much larger effort has been devoted to the understanding of their basic semiconductor properties with beneficial consequences for PV technologies.

Cu-based chalcopyrite semiconductors of the form $\text{Cu}(\text{Ga},\text{In})(\text{S},\text{Se})_2$ (CIGS) have already gained a reputation as the leading candidates for second generation photovoltaics, with the highest efficiency among thin-film solar cells (20,1%) (Jackson et al. 2011; Repins et al. 2008). This is possible thanks to the peculiar optical and structural properties of CIGS, which possess an extraordinary stability under operating conditions (Rau and Schock 1999), contrary to their binary analogue Cu_2S (Partain et al. 1983). In fact, these materials conserve to a very high degree their electronic properties in a large non-stoichiometric range and are remarkably insensitive to radiation damage or impurities. This appears to be a consequence of self-healing mechanisms that compensate for the creation of defects (Guillemoles et al. 2000; Vidal et al. 2010a). Such stability, together with direct gaps and high absorption coefficients

at the absorption edge, make them ideal PV materials.

Another class of chalcogenides shares with chalcopyrite CIGS their excellent electronic properties. It is the family of quaternary $\text{Cu}_2\text{ZnSn}(\text{S},\text{Se})_4$ (CZTS) with kesterite or stannite structure. CZTS have an extra advantage: they are only composed of elements that are naturally abundant and non-toxic. Similarly to CIGS, the alloys $\text{Cu}_2\text{ZnSnS}_x\text{Se}_{1-x}$ have optimal gaps for PV conversion, according to the Shockley-Queisser limit, and high absorption coefficients. Their use as absorbers in thin film solar cells is getting established with a growing energy conversion efficiency (almost 10% (Redinger et al. 2011; Todorov et al. 2010) for lab cells). However, the understanding of the properties of the different phases is still rather superficial.

The quest for improving the efficiency of energy conversion does not concern only the absorbing layer. Another source of loss of efficiency is the front contact of the device, made of a transparent conducting oxide (TCOs). These are insulating oxides that, for a certain range of doping, become conductive while retaining transparency in the visible spectrum. The most common examples are electron (n-)doped SnO_2 , In_2O_3 , and ZnO . Hole (p-)doping of wide gap semiconductors was for long time very hard to obtain (Nakamura et al. 1992; Neugebauer and Van de Walle 1995). It is therefore not surprising that the discovery of p-doping in CuAlO_2 thin films with a carrier mobility of about $10\text{ cm}^2/(\text{V s})$ attracted great interest (Benko and Koffyberg 1984; Kawazoe et al. 1997). TCOs are key elements for different applications, including flat screens, which implies the need for a diversification of the offer in terms of chemical elements used. We will analyse here the electronic and optical properties of Cu-based transparent conductive materials belonging to the delafossite family, such as CuAlO_2 , CuGaO_2 (Ueda et al. 2001) and CuInO_2 (Yanagi et al. 2001). The latter compound is particularly interesting as it exhibits bipolar (n- and p-type) conductivity by doping with appropriate impurities and tuning the film-deposition conditions (Yanagi et al. 2001). This opens the way to the development of transparent p-n junctions, and therefore fully transparent optoelectronic devices.

1.2 First-principle methods for electronic excitations

A reliable description from first-principles of electronic excitations in complex materials starts from identifying the best theoretical approaches, that can simplify ideally both the form of the many-body Hamiltonian and the analysis of the physical quantities involved, while conserving the desired accuracy of results.

Density functional theory (DFT) (Hohenberg and Kohn 1964; Kohn and Sham 1965) was until recently the only *ab initio* tool capable to calculate the electronic states of materials with a large number of electrons in the unit cell (see Chapter 1). However, standard DFT is designed to access ground-state properties and not excited states. This restriction is not a question of available approximations. In fact, even if one could calculate the exact Kohn-Sham (KS) eigenvalues, their differences would not necessarily be close to

measured excitation energies. Neither, by definition, they stand for electron addition or removal energies (Godby et al. 1987). Hence, the fact that the KS gap is in general reported to be too small with respect to measured gaps does not tell us *a priori* anything about the quality of a chosen approximation for the exchange-correlation potential appearing in the KS equations.

The case of materials with localized *d* or *f* states is particularly delicate. In fact, the most common approximations for the exchange-correlation functional (e.g., the local density approximation – LDA (Kohn and Sham 1965) and generalized gradient approximations – GGAs Perdew et al. (1996)), that are known to be reliable for the ground-state properties of *sp* semiconductors, may become inadequate for system with *d* or *f* electrons. In the case of the Cu-based compounds we are interested in, this problem can be traced to a poor description of the hybridization of the *d* states of the transition metal with the *p* states of S, Se and O close to the Fermi level, leading to remarkably large errors in the evaluation of bonding lengths. As a consequence, also ground state properties, such as the equilibrium atomic structure or phonon frequencies can be unsatisfactorily described by standard density functionals.

Another strong reason to go beyond DFT and its standard approximations remains the need to calculate excited states for applications in the domain of photovoltaics, i.e. to evaluate quasiparticle energies, absorption spectra, excitonic binding energies, etc. A possible solution consists in studying particle propagations and fluctuations in the system. This gives correlation functions that can then be related to response functions yielding, e.g., the linear response for optical absorption. These correlation functions are one- or two-body Green's function (Fetter and Walecka 1971). The one-body Green's function (that can essentially be understood as a time-dependent particle and hole density matrix) has phase fluctuations (i.e., poles in frequency space) given by electron addition and removal energies (quasiparticle energies), measured in photoemission or inverse photoemission experiments. The particle-hole part of the two-particle Green's function has instead poles at the energies of neutral excitations. Many-body perturbation theory (MBPT) yields a framework where one can find suitable approximations for those Green's functions. In particular, the *GW* approximation, introduced in 1965 by Lars Hedin (Hedin 1965), has been extremely successful in describing quasiparticle energies for metals, semiconductors and insulators, in the bulk as well as at surfaces and in confined structures. Restricted self-consistent procedures within the *GW* approximation (Bruneval et al. 2006a; Faleev et al. 2004; van Schilfgaarde et al. 2006) have been recently proposed and used with success for transition metal compounds, where perturbative *GW* fails. Using MBPT, the price to pay for a physically intuitive and in general quite reliable description is the high computational cost, because now Green's functions appear instead of the electronic density. In view of that, more efficient (and less reliable) approaches, often dependent on some empirical parameters, such as DFT+*U* (Anisimov et al. 1991), DFT-corrected methods (Lany and Zunger 2008; Zunger 2003), hybrid functionals (Brothers et al. 2008; Ernzerhof and Scuseria 1999; Seidl et al. 1996), have been extensively explored for the past years to

calculate electronic band structures with a reduced computational effort.

Concerning neutral excitations, the Bethe-Salpeter Equation (BSE) within MBPT is the state-of-the-art approximation (Fetter and Walecka 1971; Hanke 1978; Onida et al. 2002; Sham and Rice 1966). Another possible path to access neutral excitations, closer to the spirit of DFT, consists in actually exposing (in the computer) the system to a time-dependent external potential and calculating the evolution of the density in time. This route has become accessible thanks to the extension of DFT to its time-dependent formulation (TDDFT) (Gross and Kohn 1985, 1986; Runge and Gross 1984; van Leeuwen 2001; Zangwill and Soven 1980), put on rigorous basis by the Runge-Gross theorem (Runge and Gross 1984). By analogy to the case of classical mechanics, one can intuitively understand that in TDDFT the quantum-mechanical “trajectory” of the system under the influence of a time-dependent external potential is found by searching for the extrema of an action, instead of the minimization of a total energy, as done for the ground state. One obtains hence the time-dependent KS equations as a generalization of the static case, and from these, the response functions describing neutral excitations of a system (Petersilka et al. 1996). At this point the non-trivial difficulty resides in finding appropriate approximations for the time-dependent exchange-correlation potential $v_{xc}[n](\mathbf{r}, t)$. Note that the functional dependence is on the density in the whole space and at all past times. In particular, simple adiabatic approximations based on the static functionals proved to work particularly bad for solids (Botti et al. 2007).

Thanks to many recent developments of improved linear response kernels derived from MBPT (Adragna et al. 2003; Botti et al. 2004; Marini et al. 2003; Reining et al. 2002; Sharma et al. 2011; Sottile et al. 2003; Stubner et al. 2004; von Barth et al. 2005), TDDFT is today a real alternative to MBPT for the calculation of electronic spectra, even for solids, especially when the number of atoms in the unit cells is large and the solution of the BSE becomes unfeasible.

In this section we give a brief review of these theoretical approaches.

1.2.1 Hedin’s equations and the *GW* approximation

The time-ordered one-particle Green’s function is defined as

$$G(1, 2) = -i\langle\Psi_0|T[\hat{\psi}(1)\hat{\psi}^\dagger(2)]|\Psi_0\rangle, \quad (1.1)$$

where $|\Psi_0\rangle$ is the many-body N -particle ground state, $\hat{\psi}(1)$ [$\hat{\psi}^\dagger(1)$] is the annihilation (creation) operator of an electron in the Heisenberg picture, T is the time-ordering operator and $1 = \{\mathbf{r}_1, t_1, \sigma_1\}$ stands for the set of the real space and time coordinates plus the spin degree of freedom. The Green’s function G has poles at the frequencies of electron addition and removal energies.

The time evolution of G corresponds to the propagation of an electron (or a hole) and obeys:

$$\left[i\frac{\partial}{\partial t_1} + \frac{\nabla^2}{2} - V_{\text{ext}}\right]G(1, 2) = \delta(1, 2) - i\int d3 v(1, 3)G_2(1, 3, 2, 3^+) \quad (1.2)$$

where v is the bare Coulomb potential, V_{ext} is an external potential and the two-particle Green's function G_2 describes the creation and annihilation of pairs of particles. The equation of motion (1.2) tells us how a moving charged particle polarizes the system creating electron-hole pairs along its way. That is the reason why the two-particle quantity G_2 is involved in (1.2). In order to derive the equations of motion for G_2 , G_3 , and higher order Green's functions must be considered analogously. The hierarchy of equations containing Green's functions of increasing order can be evaluated using diagrammatic expansions based on Wick's theorem. Alternatively, one can use Schwinger's functional derivatives to obtain a set of equations for G that can be further approximated. Here we follow the second line to give a brief summary of the *GW* formalism developed in its present form by Lars Hedin (Hedin 1965).

Even though G is still unknown, (1.2) tells us that its evolution involves the polarization of the system (i.e., G_2). The physical idea at the heart of Schwinger's formalism is that the very polarization can be created as a response to a time-dependent perturbing external potential U . In the spirit of the linear-response theory, the time-dependent part of the potential will be made to vanish at the end of the derivation, so that $U \rightarrow V_{\text{ext}}(\mathbf{r})$ at $\pm\infty$. To apply this idea, the one-particle term of the Hamiltonian in (1.2), namely $h_0 = -\frac{\nabla^2}{2} + V_{\text{ext}}$, becomes $h_0 = -\frac{\nabla^2}{2} + U$.

It is possible to show that the variation of G with respect to U gives:

$$\frac{\delta G(1, 2)}{\delta U(3)} = G(1, 2)G(3, 3^+) - G_2(1, 3, 2, 3^+). \quad (1.3)$$

Using (1.3), the equation of motion (1.2) reads

$$\left[i \frac{\partial}{\partial t_1} - h_0(1) + i \int d3 v(1, 3)G(3, 3^+) \right] G(1, 2) = \delta(1, 2) + i \int d3 v(1^+, 3) \frac{\delta G(1, 2)}{\delta U(3)}. \quad (1.4)$$

where the two-particle Green's function does not appear anymore. As $-iG(3, 3^+) = \rho(3)$, where ρ is the electronic density, the term $-i \int d3 v(1, 3)G(3, 3^+)$ is nothing more than the Hartree potential $V_{\text{H}}(1)$. This means that the effects of the perturbation U on the system can be split into a classical contribution (i.e., the Hartree term) and the contribution that encompasses quantum effects. The latter term can be rewritten by defining the self-energy Σ :

$$i \int d3 v(1^+, 3) \frac{\delta G(1, 2)}{\delta U(3)} = \int d3 \Sigma(1, 3)G(3, 2). \quad (1.5)$$

The self-energy therefore plays the role of a non-local and dynamical potential that accounts for all the effects of exchange and correlation in the system. Physically, it represent the effective potential that an extra fermion in the system feels for the polarization that its propagation induces due to exchange effects. Using (1.5) in (1.2) one obtains:

$$\left[i \frac{\partial}{\partial t_1} - h_0(1) - V_{\text{H}}(1) \right] G(1, 2) = \delta(1, 2) + \int d3 \Sigma(1, 3)G(3, 2). \quad (1.6)$$

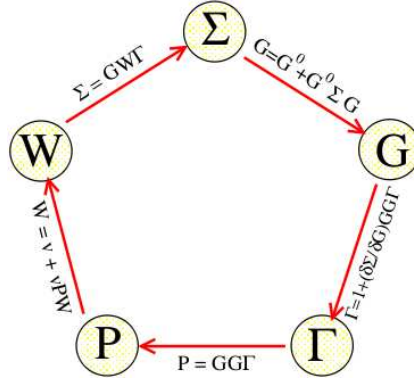


Figure 1.2 Hedin's pentagon connecting the Green's function G , the self-energy Σ , the vertex Γ , the polarizability P and the screened Coulomb interaction W .

Setting $\Sigma = 0$ in (1.6), it is possible to define the Hartree Green's function G_H , which is the resolvent of the Hartree Hamiltonian calculated with the exact electronic density ρ :

$$\left[i \frac{\partial}{\partial t_1} - h_0(1) - V_H(1) \right] G_H(1, 2) = \delta(1, 2). \quad (1.7)$$

Combining (1.6) and (1.7) one finds the Dyson equation for G :

$$G(1, 2) = G_H(1, 2) + \int d^3 4 G_H(1, 3) \Sigma(3, 4) G(4, 2). \quad (1.8)$$

The self-energy is responsible for the renormalization effect that yields the difference between the propagation of an independent (Hartree) particle and the propagation of an interacting fermionic particle.

From (1.5) one can then extract with a little of algebra a definition of Σ of practical use:

$$\Sigma(1, 2) = i \int d^3 4 G(1, 4) \Gamma(4, 2; 5) \frac{\delta V(5)}{\delta U(3)} v(3, 1^+). \quad (1.9)$$

where $V(1) = U(1) + V_H(1)$ is the total classical potential, and where the irreducible vertex function has been introduced:

$$\Gamma(1, 2; 3) = -\frac{\delta G^{-1}(1, 2)}{\delta V(3)} = \delta(1, 3) \delta(2, 3) + \frac{\delta \Sigma(1, 2)}{\delta V(3)}. \quad (1.10)$$

The derivative $\delta \Sigma / \delta V$ is then usually replaced by the chain rule $(\delta \Sigma / \delta G)(\delta G / \delta V)$ and (1.10) is transformed into an integral equation:

$$\Gamma(1, 2; 3) = \delta(1, 2) \delta(1, 3) + \int d^4 5 6 7 \frac{\delta \Sigma(1, 2)}{\delta G(4, 5)} G(4, 6) G(7, 5) \Gamma(6, 7; 3). \quad (1.11)$$

Following a strictly analogous procedure one obtains also the equations:

$$\Sigma(1, 2) = i \int d34 G(1, 3) \Gamma(3, 2; 4) W(4, 1), \quad (1.12)$$

$$W(1, 2) = v(1, 2) + \int d34 v(1, 3) P(3, 4) W(4, 2), \quad (1.13)$$

$$P(1, 2) = -i \int d34 G(1, 3) G(4, 1) \Gamma(3, 4; 2), \quad (1.14)$$

in terms of the time-ordered polarization operator $P(1, 2)$ and the dynamical screened interaction $W(1, 2) = \delta V(1) / \delta U(3) v(3, 2) = \epsilon^{-1}(1, 3) v(3, 2)$. Equations (1.8), (1.11), (1.12), (1.13), (1.14) form the closed set of five equations known as Hedin's equations. They depend on one another and should be solved iteratively following the scheme of Fig. 1.2.

The "famous" *GW* approximation is obtained by disregarding the second term on the right-hand side of (1.11) and inserting Γ in (1.12):

$$\Gamma(1, 2; 3) = \delta(1, 2) \delta(1, 3), \quad (1.15)$$

$$\Sigma(1, 2) = i G(1, 2) W(2, 1). \quad (1.16)$$

Going beyond the *GW* approximation requires the inclusion of vertex corrections, by solving (1.11) with its four-point kernel dominated by $\delta \Sigma(1, 2) / \delta G(3, 4)$. Indeed, (1.11) is the main obstacle to the calculation of polarizabilities and self-energies beyond the RPA and the *GW* approximation.

The main plus of the *GW* approach is that polarization effects, that screen the propagation of an extra particle, are explicitly taken into account through a dynamically screened self-energy. Instead, in Hartree-Fock there is no polarization and no relaxation of the system and the self-energy is static. Even if vertex corrections are neglected and the self-energy is evaluated within the *GW* approximation, the Dyson equation 1.8 is still a self-consistent equation in G and should be solved iteratively. In this sense the starting point is arbitrary. In fact, it is possible to start with Green's functions of any non-interacting system and iterate self-consistently (keeping the vertex $\Gamma = 1$).

Even if Hedin obtained the *GW* approximation by iterating Hedin's equations starting from $\Sigma = 0$, i.e., from the Hartree Green's function, modern calculations (starting from the works of Strinati et al. (1982), Hybertsen and Louie (1985, 1986) and Godby et al. (1987, 1988)) use rather a "best G , best W " approach (Del Sole et al. 1994). This means that the idea of a strict iterative solution of Hedin's equations is dismissed, and the *GW* self-energy is constructed instead using the best mean-field results that are available. The simplest choice is in general to use the KS eigenvalues and eigenfunctions coming from a DFT calculation within LDA or GGA. We will refer to this procedure as perturbative *GW*.

It is clear that a perturbative approach is justified when the departure wavefunctions are already close to the quasiparticle ones. This is indeed the case for many systems, and therefore perturbative *GW* has been extremely successful in

describing electron addition and removal energies for metals, semiconductors and insulators (Aulbur et al. 1999). However, perturbative *GW* has also proved to be insufficient for many transition metal compounds (Bruneval et al. 2006a,b; Gatti et al. 2007; Kammerlander et al. 2011; van Schilfgaarde et al. 2006; Vidal et al. 2010a,b). The problem in many cases is that the LDA wave-functions are not localized enough, leading even to an artificial metallic character in materials that are insulators. Perturbative *GW* may already improve upon this situation by opening the gap, but usually by an insufficient amount.

Several methods have appeared for the recent years to solve this problem. They follow two main lines: i) Replacing the simple LDA with a better starting point and then performing a single-shot *GW* calculation. Several attempts to improve the starting point with respect to LDA can be found in the literature, like using GGA (Li et al. 2002), exact exchange (Rinke et al. 2005), LDA/GGA+U (Jiang et al. 2009; Kioupakis et al. 2008) or hybrid functionals (Fuchs and Bechstedt 2008). ii) Performing (restricted) self-consistent (sc) *GW* (Bruneval et al. 2006a; Faleev et al. 2004; van Schilfgaarde et al. 2006). The technique proposed by Faleev et al. (2004) is called quasiparticle sc*GW* and has the advantage of being independent of the starting point (obviously at the price of a larger computational complexity). There is an alternative self-consistent procedure, that yields wavefunctions extremely close to those obtained in a quasiparticle sc*GW* calculation at a reduced computational cost: this method is sc-COHSEX, as explained by Bruneval et al. (2006a). The dynamical effects that are absent in COHSEX calculations can then be accounted for by performing a final perturbative *GW* step starting from the scCOHSEX result. scCOHSEX+ G_0W_0 has already been applied to many transition metal compounds, yielding excellent results for the band gaps and the quasiparticle band structure (Bruneval et al. 2006a,b; Gatti et al. 2007; Kammerlander et al. 2011; Vidal et al. 2010a). Note that whenever compared, quasiparticle sc*GW* and scCOHSEX+ G_0W_0 gave very similar band gaps and wavefunctions.

1.2.2 Hybrid functionals

Even in its perturbative form, *GW* is by all measures an expensive technique, with a very unfavorable scaling with the number of atoms in the unit cell. It is therefore unpractical for the study of band structures of large systems and prohibitive to obtain total energies even for simple realistic systems. Much of the computational effort in *GW* comes from the dynamically screened Coulomb interaction W . It is therefore interesting to explore to which extent dynamical effects are mandatory, or whether non-locality is the dominating characteristic. The move from local KS potentials to non-local functionals has first been pushed forward in Quantum Chemistry, where today the so-called hybrid functionals are very popular. These functionals mix a fraction α of Fock exchange with a combination of LDA and generalized gradient (GGA) functionals. The application of hybrid functionals to the solid state had a slower start (Brothers et al. 2008; Ernzerhof and Scuseria 1999). The

situation changed recently, helped by the wider availability of computer codes that support hybrids (Kresse and Furthmüller 1996a; Kresse and Furthmüller 1996b) and the steady increase of computational power covering the additional cost with respect to a local potential. Besides yielding good structural properties (Paier et al. 2007) hybrids have proved to correct to a large extent the bandgap problem (Brothers et al. 2008; Paier et al. 2008). Another landmark came with the introduction of screened hybrids (Heyd et al. 2003, 2006). These functionals lead to faster calculations and improved bandgaps, especially for small bandgap systems. Furthermore, by screening the Coulomb interaction at large distances, they also give access to metals.

The intuition lying behind a hybrid functional is rather clear. While LDA or GGA calculations strongly underestimate the gap, Hartree-Fock calculations overestimate it typically by more than a factor of two. By changing the mixing α from 0 to 1, one has a continuous change between local KS and Hartree-Fock, and an essentially linear variation between the respective gaps. Therefore, to obtain the experimental gap one simply has to use the appropriate mixing parameter. This value can be determined from a fit to a series of systems, and is often set to around $\alpha \sim 0.2 - 0.3$. This choice gives very good results for a large class of systems, but it usually fails when the gap is very large or very small. This fact is easy to understand if we move away from a generalized KS picture (Seidl et al. 1996), and consider the hybrid as an approximation to the self-energy Σ . In the GW approximation the latter can be written as

$$\Sigma(\mathbf{r}, \mathbf{r}'; \omega) = \Sigma_{\text{sX}}(\mathbf{r}, \mathbf{r}') + \Sigma_{\text{rest}}(\mathbf{r}, \mathbf{r}'; \omega), \quad (1.17)$$

with $\Sigma_{\text{sX}}(\mathbf{r}, \mathbf{r}')$ being the statically screened-exchange (sX) term, and $\Sigma_{\text{rest}}(\mathbf{r}, \mathbf{r}'; \omega)$ containing the static Coulomb hole and dynamical contributions. If the screening in the sX term is replaced by an effective static dielectric constant $\epsilon_{\infty} = 1/\alpha$, and Σ_{rest} is modeled by the static and local part of the hybrid functional (Gygi and Baldereschi 1989), the quasi-particle equation has the same form as the generalized KS equation solved for hybrid functionals. Note that this is similar to the sX LDA method (Bylander and Kleinman 1990; Clark and Robertson 2010; Seidl et al. 1996), where Σ is replaced by a Thomas-Fermi-screened exchange part and the LDA xc functional. From these arguments we can conclude that the physical value for the mixing parameter α is related to the inverse of the dielectric constant of the material at hand (Alkauskas et al. 2010; Marques et al. 2011; Vidal et al. 2010a).

At present, hybrid functional calculations are more and more common in theoretical studies for photovoltaics, as they offer a very good compromise between accuracy and efficiency. In particular, band gaps of the order of 1–2 eV are included in the ideal window (Marques et al. 2011) for reliable band gap calculations using screened-hybrids, such as HSE06. However, a major problem still remains, related to the use of one single mixing parameter for all materials, resulting in significant errors of traditional hybrid functionals for large and small gap materials. Nevertheless, hybrid functionals represent for the time being the only possible way to study electronic excitations in systems with large unit cells (such as supercells containing hundreds of atoms to describe defects),

which explains the interest for finding improved functionals Marques et al. (2011).

1.2.3 The Bethe-Salpeter equation

Band structures and photoemission experiments are based on a description in terms of a one-particle effective Hamiltonian for one-particle excitations, i.e. quasiparticles. In case of absorption experiments, instead, a one-particle description is no longer adequate, since one has to deal with the simultaneous creation of a quasidelectron and a quasihole which interact in the system. In this section we will therefore introduce the effective two-particle Hamiltonian capable of dealing with these neutral excitations.

The BSE uses the intuitive scheme of MBPT, which makes the task to identify efficient approximations easier. The key quantity is the four-point reducible polarizability L , that can be expressed in terms of two-particle Green's function G_2 describing the propagation of two particles (for absorption, the relevant part describes the propagation of an electron and a hole):

$$L(1, 2, 3, 4) = L_0(1, 2, 3, 4) - G_2(1, 2, 3, 4), \quad (1.18)$$

where L_0 is the disconnected part consisting of two one-particle Green's functions G :

$$L_0(1, 2, 3, 4) = iG(1, 3)G(4, 2). \quad (1.19)$$

The function L satisfies a Dyson-like screening equation, known as the Bethe-Salpeter equation:

$$L(1, 2, 3, 4) = L_0(1, 2, 3, 4) + \int d5678 L_0(1, 2, 5, 6) [v(5, 7)\delta(5, 6)\delta(7, 8) + \Xi(5, 6, 7, 8)] L(7, 8, 3, 4). \quad (1.20)$$

In order to solve (1.20) one has to approximate the many-body interaction kernel Ξ . The standard approximation consists in using the *GW* self-energy of (1.16). In this way the solution of the BSE corresponds to the inclusion of vertex corrections in P through a second iteration of Hedin's pentagon of equations. When the BS kernel is approximated to first order in the screened Coulomb interaction W , the BSE reads:

$$L = L_0 + L_0 ({}^4v - {}^4W) L. \quad (1.21a)$$

In (1.20) we have defined the four-point extension of the Coulomb potential ${}^4v(1, 2, 3, 4) = \delta(1, 2)\delta(3, 4)v(1, 3)$, whereas ${}^4W = \delta(1, 3)\delta(2, 4)W(1, 2)$ is the four-point extension of the screened Coulomb potential. The first term, the unscreened electron-hole exchange, is repulsive, while the second term, the screened electron-hole Coulomb interaction, is attractive. Note that the δ -functions connect different indices in the two cases: this is due to the fact that the former stems from variations of the Hartree potential, whereas the latter is due to variations of an exchange-like self-energy contribution. Because of the way the indices are connected in this second case, the BSE can not be

written in a two-point form. This issue represents the real bottleneck in practical calculations. Instead, the measurable response function is obtained via a two-point contraction of L , namely

$$P^{\text{red}}(1, 2) = -L(1, 1, 2, 2). \quad (1.22)$$

From the reduced polarizability P^{red} that is understood to be time- (or contour-) ordered, the causal response function χ can be inferred; the relation between the time-ordered and causal response is in fact $\chi(\omega > 0) = P^{\text{red}}(\omega > 0)$. Another useful quantity is the independent quasi-particle polarizability, $P_0(1, 2) = -L_0(1, 1, 2, 2)$. Note that this is not equal to $\chi_{\text{KS}} = -iG_{\text{KS}}G_{\text{KS}}$. The expression looks similar, but the KS states and eigenvalues in χ_{KS} are now replaced by their MBPT counterparts, which are, at this level of approximation, determined in the quasi-particle *GW* approximation (Hedin 1965). To be precise, practical calculations use *GW* eigenvalues and KS wavefunctions to build G .

For simple semiconductors, dynamical effects in the electron-hole screening in W and in the Green's function G tend to cancel, therefore they are usually neglected in both terms. This means that, instead of $W(1, 2)$ one uses a statically screened instantaneous interaction and for G the Green's function obtained by a perturbative or *scGW* calculation. In practice, the BSE (1.20) is solved by diagonalizing a two-particle excitonic Hamiltonian, providing information about the excitonic eigenstates and eigenvalues. The BSE yields excellent results for the optical properties of solids with both continuum and bound excitons, in bulk and nanostructured system (Onida et al. 2002).

1.2.4 Model kernels for TDDFT

Whenever the solution of the BSE is unfeasible, it is however possible to identify efficient ways to calculate absorption spectra, going beyond the simple sum over independent-transitions between KS states. An appealing idea is to use the time-dependent (TD) generalization of DFT: TDDFT (Gross et al. 1996; Runge and Gross 1984), whose central quantity is the electronic density that responds to a time-dependent external field. TDDFT retains all the advantages of the DFT formalism in terms of computational efficiency. However, the lack of good approximations for the time-dependent exchange-correlation (xc) functional, especially in the case of solids (Botti et al. 2007; Onida et al. 2002), is its principal limitation.

The exchange-correlation kernel f_{xc} of TDDFT, which is the variation of the exchange-correlation potential with respect to the electronic density, is most often approximated by (i) $f_{\text{xc}} = 0$, leading to the random-phase approximation (RPA), or (ii) $f_{\text{xc}} = \delta v_{\text{xc}}^{\text{LDA}} / \delta \rho$, which gives the adiabatic local-density approximation (Gross et al. 1996; Zangwill and Soven 1980) (ALDA). Note that the RPA differs from an independent-particle calculation, even if the xc kernel is zero, because it accounts for variations of the Hartree-potential upon excitation. This is a classical contribution, which in the optical spectra corresponds to local field or depolarization effects, particularly important when charge inhomogeneities are pronounced.

Concerning the calculation of absorption spectra of semiconductors, neither the RPA nor the ALDA are sufficient to yield results in quantitative (and sometimes not even in qualitative) agreement with experiments. In particular, the lack of a long-range ($1/r$) decay of the ALDA linear response kernel f_{xc} can cause large errors in the calculation of absorption spectra of extended systems (Botti et al. 2007; Gonze et al. 1995; Onida et al. 2002). Nevertheless, it has been shown (Botti et al. 2007; Reining et al. 2002) that in some cases an agreement with experiments can be recovered by retaining only the long-range contribution (LRC) that the exact f_{xc} should have in the asymptotic limit. In the following we will see an example of resulting model kernels Botti et al. (2005, 2004) accounts for continuum excitonic effects, giving very good optical properties for small-medium gap semiconductors, with a computational burden comparable to a DFT approach.

One should remember however that CIGS materials possess bound excitons (Bellabarba et al. 1996; Levchenko et al. 2007; Ringeissen et al. 1973; Tell and Kasper 1973), and that the TDDFT-LRC approach has proved to work better for systems with continuum excitons. That is why the only fully reliable approach in this case is the solution of the computationally demanding BSE or the use of a more sophisticated model kernel, which describes accurately the electron-hole pair dynamics (Adragna et al. 2003; Marini et al. 2003; Sharma et al. 2011; Sottile et al. 2003). Nevertheless, the simple model kernels remain often the best compromise between accuracy and efficiency whenever one wants to deal with large supercells to study interfaces or defects.

1.3 Examples of applications

The first-principle approaches presented in Sec. 1.2 have recently been applied for the first time to complex materials of technological interest. In this chapter we select three illustrative applications of self-consistent *GW* in the field of photovoltaic energy conversion, where the use of accurate state-of-the-art methods has allowed to clarify controversial results in literature.

Our first example concerns copper indium/gallium diselenide/disulfide $\text{Cu}(\text{In,Ga})(\text{Se,S})_2$ (CIGS) compounds. These materials are doped by native defects. These defects play an important role in the definition of the exceptional stability under operating conditions of the electronic properties of these compounds. We will discuss more in detail here the effect of Cu vacancies.

The second example are kesterite and stannite $\text{Cu}_2\text{ZnSnS}_4$ compounds. This family of quaternary chalcogenide is emerging as an alternative to CIGS materials, and share with the parent family extraordinary structural and electronic properties.

The third example is the family of $\text{Cu}(\text{Al,In,Ga})\text{O}_2$ delafossite transparent conductive oxides, which possess a chemical composition similar to CIGS compounds. A long-standing debate on the direct and indirect fundamental gaps of these materials has intrigued for years experimentalists and theoreticians.

Concerning the calculations discussed in Sec. 1.3, the set of methods used includes DFT in the standard LDA and GGA, LDA/GGA+*U*, hybrid functionals

and *GW* approaches. The reported standard DFT and *GW* calculations were performed within the plane-wave scheme implemented in ABINIT (Gonze et al. 2005), using norm-conserving pseudopotentials (Troullier and Martins 1991) and including semi-core states in the valence. Hybrid functional and LDA/GGA+*U* calculations were performed with the Vienna ab initio simulation package (VASP) (Blöchl 1994; Kresse and Furthmüller 1996a; Kresse and Furthmüller 1996b; Kresse and Joubert 1999). TDDFT and BSE spectra were obtained using the code YAMBO (Marini et al. 2009). More details on calculations can be obtained in the cited references.

1.3.1 *Cu-based thin-film absorbers*

Ternary chalcopyrites crystals are obtained from the zincblende structure by replacing the Zn cations alternatively with Cu and In or Ga. $\text{CuIn}(\text{S,Se})_2$ compounds are commonly referred to as CIS and $\text{CuGa}(\text{S,Se})_2$ compounds are known as CGS. The two families together are the so-called CIGS materials. In ternary chalcopyrites each anion (Se or S) is coordinated by two In or Ga and two Cu atoms, while each cation is tetrahedrally coordinated by four anions. The existence of two different cations results in two different bonding lengths $R_{(\text{In,Ga})-(\text{S,Se})}$ and $R_{\text{Cu}-(\text{S,Se})}$, leading to two structural anomalies (Jaffe and Zunger 1984): i) The tetragonal cell exhibits a distortion, defined by the parameter $\eta = c/2a \neq 1$, the ratio between the lattice constants a and c . ii) The ideal zincblende site for the anion is perturbed, yielding a deformation of the anion tetrahedron, which is measured by the anion displacement parameter

$$u = \frac{1}{4} + \left[R_{\text{Cu}-(\text{S,Se})}^2 - R_{(\text{In,Ga})-(\text{S,Se})}^2 \right] / a^2 \neq \frac{1}{4}. \quad (1.23)$$

Both structural anomalies are small, but not negligible. The precise experimental determination of the anion displacement u is more difficult than the measurement of the lattice constants a and c due to the inhomogeneity of the samples. Indeed, the dispersion of the measured values is very small for the lattice parameters (usually $< 1\%$), while it is significant (as large as 7%) for the anion displacement (Jaffe and Zunger 1984; Merino et al. 1996).

Merino et al. (1996) reported a relatively narrow spread in the band gap ($\approx 10\%$) as a function of the dispersion of the anion displacement u . This finding is coherent with the observation of an extraordinary stability of CIGS absorbers under operating conditions. Unfortunately, experiments alone are not conclusive, due to the lack of information on the composition and uniformity of the samples. In fact, in real samples there is a dispersion of values of u . It is therefore interesting to calculate the evolution of the gaps as a function of u . This was first addressed theoretically using DFT (Jaffe and Zunger 1983), in some cases including empirical corrections to get closer to the experimental gap (Jaffe and Zunger 1984; Jiang and Feng 2008). An uncommonly large variation was found, in apparent contradiction with the experimentally proved insensitivity of the CIGS gap to any kind of damage or perturbation.

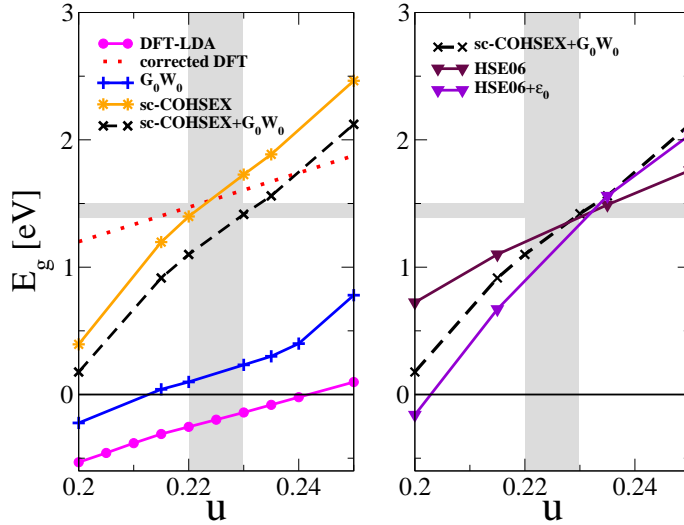


Figure 1.3 Photoemission band gap versus the anion displacement u for CuInS_2 . The vertical shaded areas give the spread of experimental data for u , while the horizontal shaded areas give the dispersion of measured band gaps. Left panel: calculations using DFT-LDA, G_0W_0 , scCOHSEX, and scCOHSEX+ G_0W_0 . The dotted line refer to the work of Jiang and Feng (2008). Right panel: comparison of scCOHSEX+ G_0W_0 and hybrid functional calculations, using HSE06 and a modified HSE06. From Vidal et al. (2010a)

In the following we will focus on CIS materials, in particular using CuInS_2 as a test case. Similar results were found for CuInSe_2 , CuGaSe_2 and CuGaS_2 (Aguilera et al. 2011; Vidal et al. 2010a). A first question to answer is if the DFT data can be trusted, as they were obtained from KS eigenvalues using LDA or GGA functionals. Indeed, these approximations are known to perform badly in CIGS materials. For example, in CIS the KS band gap is vanishing, in contrast to the experimental values of 1.54 eV and 1.05 eV for CuInS_2 and CuInSe_2 (Alonso et al. 2001), respectively. Moreover, *ad hoc* corrections, like the scissor operator, often used to adjust the DFT band gap to the experimental value, are too simplistic to analyze the dependence of the band gap on u .

In spite of the underestimation of the band gap, LDA and GGA usually yield good structural parameters for semiconductors and insulators. Unfortunately, for CIS, the theoretical range of anion displacements obtained within these approximations ($0.215 < u < 0.220$) lies outside the experimental range. It is clear, thus, that to understand the paradox of the band gap dependence on the unit cell deformations in CIGS chalcopyrites one has to go beyond standard DFT.

We have already seen that scGW and hybrid functional are the most pertinent approaches beyond standard DFT. These approaches were applied by Vidal et al. (2010a) to study the interplay between structural and electronic properties in CIS compounds. Here we analyse the main findings of that work, in comparison with previous experimental and theoretical results.

If the atomic arrangement in the unit cell is relaxed using LDA or GGA functionals the anion displacement u is systematically underestimated by 5-10%, in agreement with previous results (Domain et al. 2003; Jaffe and Zunger 1983; Łazewski et al. 2002). Moreover, always within LDA/GGA, the KS bottom conduction band overlaps the KS top valence band, yielding negative band gaps (Wei and Zunger 1988). On the other hand, values of u in agreement with experiments can be obtained using the Heyd-Scuseria-Ernzerhof (HSE06) (Heyd et al. 2003) hybrid functional (Vidal et al. 2010a). In fact, the structural relaxation within HSE06 yields $u=0.226$ ($u=0.229$) for the ideal monocrystal of CuInS_2 (CuInSe_2). HSE06 gives slightly underestimated band gaps for CIGS. Band gaps in excellent agreement with experiments are obtained from *scGW* once that the experimental geometry (or the HSE06 geometry) is fixed. Unfortunately, *scGW* cannot be used to perform structural relaxations.

In order to study the variations of the gap upon structural distortion, Vidal et al. (2010a) varied u in the interval $0.2 < u < 0.25$ that encompasses both experimental and theoretical ranges, and evaluated the quasiparticle band structures using and comparing different *ab initio* schemes. They also verified that sensible variations of the lattice parameters a and c have negligible effects on the gap.

The dependence on u of the band gap of CuInS_2 is shown in Fig. 1.3 Vidal et al. (2010a). We can see that the KS-LDA curve (magenta with filled circles) has the same slope as the theoretical curve (dotted line) obtained by Jiang and Feng (2008) using the LDA corrected by a scissor operator. By applying the perturbative G_0W_0 approach on top of DFT (blue line with crosses), bands are reordered, reversing the sign of the band gap for $u > 0.215$. In any case, G_0W_0 gaps remain quite small, and the slope of the curve does not change for most of the u -range when compared to the KS results. The slope of the G_0W_0 calculation increases when $u = 0.25$, becoming comparable to the slope of the curves obtained applying a self-consistent approach. This is the only case for which the KS gap is already positive and no band reordering occurs.

The *scCOHSEX* procedure (yellow lines with stars) leads to a very different result: the gap enlarges (to values slightly larger than the experimental ones), and also the slope of the curve significantly increases. This is due to the progressive modification in the self-consistent iterations of the unsatisfactory LDA starting point. When the *scCOHSEX* eigenstates are used as a starting point for a perturbative G_0W_0 calculation (black dashed lines), the band gap gets reduced by a constant value of about 0.3 eV, without affecting the slope of the dependence on u . Note that the *scCOHSEX*+ G_0W_0 band gap is in agreement with experimental data for the anion displacement measured for the monocrystal (Abrahams and Bernstein 1973).

Something more can be learnt from HSE06 calculations for the gaps (maroon line with filled triangles), that yield an intermediate slope between DFT-LDA and *scCOHSEX*+ G_0W_0 . The effect of the HSE06 functional is determined by the fixed amount of Hartree-Fock (HF) exchange included:

$$E_{\text{xc}}^{\text{HSE06}} = E_{\text{xc}}^{\text{GGA}} + \frac{1}{4}E_{\text{x}}^{\text{HF,sr}} - \frac{1}{4}E_{\text{x}}^{\text{GGA,sr}}, \quad (1.24)$$

where the exchange term $\frac{1}{4}E_{\text{HF, sr}}$ can be seen as an approximated contribution to the self-energy, whose Coulomb interaction is screened by the mixing parameter $\frac{1}{4}$ and the short-range (sr) screening factor, while $\frac{1}{4}E_{\text{x}}^{\text{GGA, sr}}$ is a screened GGA exchange. In contrast, in a *GW* calculation the exchange part of the self-energy is screened by the inverse dielectric constant, as a first approximation using the static ε_{∞} ; the latter varies for different values of u . To shed light on this point Vidal et al. (2010a) performed a series of HSE06 calculations using $\frac{1}{\varepsilon_{\infty}}$, computed for each value of u , to replace the mixing parameter in front of the screened Hartree-Fock exchange. The resulting curve (violet line with open triangles) has the same slope as the scCOHSEX curve, pointing to the fact that the electronic screening is the essential ingredient that controls the band gap. This idea was further exploited by Marques et al. (2011) to obtain a non-fixed mixing parameter for hybrid functionals, sensitive to screening.

Note that sc*GW* cannot be applied at the moment to supercells containing d electrons if the unit cell is larger than 20–30 atoms. As long as larger cells are out of reach for *GW* calculations, hybrid functionals, in particular with improved approximations for the mixing parameter, promise to be a computationally efficient alternative with a satisfactory degree of accuracy.

In summary, all theoretical results, independently of the level of sophistication, reveal variations of the band gap well outside the experimental range of values. In fact, considering as an upper limit for Δu the range where both theoretical and experimental values are included ($\Delta u \lesssim 0.02$), we deduce that the gap variation ΔE_{g} due to the anion displacement alone would be $\Delta E_{\text{g}} = 32.2 \times \Delta u \approx 0.65$ eV. This suggests that the puzzle of electronic stability of CIGS compounds cannot be solved simply by replacing LDA for a more accurate quasiparticle calculation.

A hint of the possible solution of this apparent paradox of band gap stability can be found by considering also the effect of high concentrations of defects (Rau and Schock 1999). Here we consider as an example the effect due to Cu vacancies V_{Cu} , shallow acceptor defects which are known to be present in all samples, consistently with the observation of p-type conductivity. In particular, V_{Cu} is thought to have very low formation energies (Zhang et al. 1998) compared to other intrinsic defects. One should not forget that other defects are known to be present in large concentrations, in particular Cu_{In} and In_{Cu} antisites, which participate in the formation of complexes of defects with very low formation energy (Zhang et al. 1998). Indeed, a complete model should include the effects of all most common defects.

Already at the KS level the presence of Cu vacancies V_{Cu} opens up the band gap (Xiao et al. 1994; Zhang et al. 1998), with a larger effect for increasing concentrations of V_{Cu} , once again in contradiction with the observed stability of experimental band gaps against stoichiometry deviations. This trend is confirmed by G_0W_0 calculations for supercells (Vidal et al. 2010a) corresponding to concentrations of V_{Cu} in the usual experimental range of off-stoichiometry (Merino et al. 1996). The concentration of V_{Cu} is related to the formation energy ΔE_{f} through a Boltzmann distribution, whose relevant temperature and chemical potentials are set by the growth conditions ($T \approx 500$ –

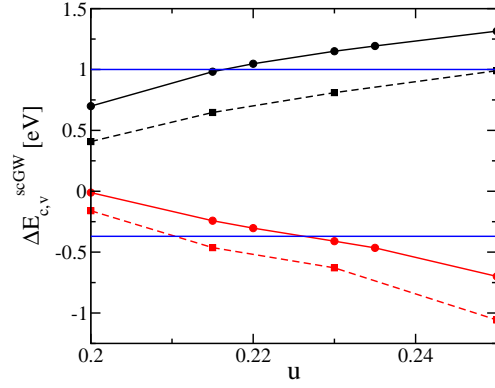


Figure 1.4 The shifts of the conduction band minimum (CBM) and valence band maximum (VBM) $\Delta E_{c,v}$ of CuInS_2 with respect to the LDA band edge versus the anion displacement u . We compare results for scCOHSEX with self-consistency only in energy (dashed curve) and in both wave functions and energies (continuous curve). The blue horizontal lines represent $\Delta E_{c,v}$ given by DFT+ U_d (Persson and Zunger 2005) where U is set to 6 eV. Modified from Vidal et al. (2010a)

600° C, copper poor samples) at which defect equilibrium occurs, this equilibrium is moreover assumed to be quenched during the rapid cool down of the samples. However, previous calculations of formation energies were done at the level of DFT and suffered from the unsatisfactory description of the localized states contributing to the VBM. Lany and Zunger (2008) proposed to use LDA+ U to correct the formation energy as follows:

$$\Delta E_f = \Delta E_f^{\text{LDA}} - \Delta E_v^{\text{LDA}+U}. \quad (1.25)$$

Vidal et al. (2010a) used this idea, evaluating the VBM shift ΔE_v within scGW. In this case, ΔE_v does not correct a shortcoming of KS theory, but improves on the LDA functional, as the exact exchange-correlation functional would give the exact VBM already within DFT. In Fig. 1.4 one can find the band edge corrections $\Delta E_{c,v}$ with respect to the KS VBM, calculated using scGW and shown for different levels of self-consistency. The VBM shift has a dispersion of around 1 eV in the considered range of u . This dispersion is totally absent in DFT (+ U) calculations (Persson and Zunger 2005) (horizontal blue line). Note that the shifts are significantly different according to whether both wave functions and eigenvalues or only eigenvalues are updated in the self-consistent procedure. Figure 1.4 proves as well that the variations of the band gap with u are due to both variations of the CBM and the VBM.

Following the logic of the feedback loop scheme of Fig. 1.5, one can realize that if a distortion of the lattice occurred for any reason (e.g. extended defect, axial strain,...) it would actually have little influence on the gap value because of two compensating effects.

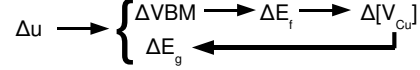


Figure 1.5 Schematic representation of the feedback-loop that stabilizes the band-gap. From Vidal et al. (2010a).

Let assume that the band gap is a functional of u and $[V_{\text{Cu}}]$ so that $E_g = E_g(u, [V_{\text{Cu}}])$. Any variation of the band gap ΔE_g can be expressed as

$$\Delta E_g = \frac{\partial E_g}{\partial u} \Delta u + \frac{\partial E_g}{\partial [V_{\text{Cu}}]} \Delta [V_{\text{Cu}}], \quad (1.26)$$

where u is the anion displacement and $[V_{\text{Cu}}]$ is the concentration of Cu vacancies. The two variables u and $[V_{\text{Cu}}]$ are in fact not independent but linked through the variation of the VBM induced by variations of u . In the case of a shallow acceptor, its formation energy should be corrected by the correct position of the VBM (see Eq. 1.25) as

$$\Delta E_f(u) = \Delta E_f^{\text{DFT}} - \Delta E_v^{\text{scGW}}(u). \quad (1.27)$$

The derivatives entering in Eq. 1.26 were calculated by fitting the curves in Fig. 1.6.

Shallow acceptors are supposed to behave like the VBM due to their proximity to it. This has been the common strategy used for the past 20 years in order to correct formation energies (see, e.g., Lany and Zunger (2008)). Then, it is possible to relate the concentration of V_{Cu} to the formation energy through a Boltzmann distribution as

$$[V_{\text{Cu}}] = N_{\text{Cu}} e^{\frac{-\Delta E_f}{k_B T}}, \quad (1.28)$$

with T being the growth temperature for which the diffusion of defects is quenched ($T \approx 500 - 600^\circ \text{C}$). Moreover, high concentrations of V_{Cu} can significantly enlarge the band gap. Thus, any variation of u can change both the band gap and the formation energy of V_{Cu} , and as a consequence vary the concentration of V_{Cu} which will change the band gap accordingly. Overall the effects of u and V_{Cu} cancel each other.

The same dependence of the gap on u was found for CGS compounds, except for the fact that the GGA values of u are inside the experimental window, due to a compensation of errors in the calculation of bond length (Aguilera et al. 2011). Analogous results are also found for quaternary CZTS compounds, whose electronic properties are extremely similar to the ones of the parent CIGS family. Let us analyse more in detail this statement. This will give us the possibility to have a closer look at the band structures obtained using the different levels of approximation.

In literature there are only few recent studies that address the structural (Botti et al. 2011; Chen et al. 2009a, 2010b; Persson 2010), electronic (Chen et al. 2009a; Paier et al. 2009; Persson 2010), and defect properties (Chen et al. 2010a; Nagoya et al. 2010) of CZTS. The zincblende-derived

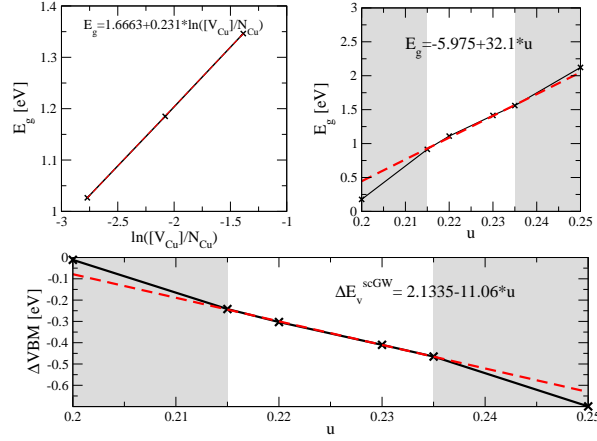


Figure 1.6 Top left panel: Value of the band gap of CuInS_2 calculated in G_0W_0 versus the concentration of Cu vacancies. Top right panel: Value of the band gap of CuInS_2 calculated in $\text{scCOHSEX}+G_0W_0$ versus the anion displacement. Bottom panel: ΔE_v^{scGW} of CuInS_2 versus the anion displacement. From Vidal et al. (2010a)

kesterite structure ($I\bar{4}$) is recognized to be the most stable. The energy difference per atom with respect to the stannite structure ($I\bar{4}2m$) is however only of few meV per atom (Chen et al. 2009a,b; Persson 2010), proving that kesterite and stannite phases can coexist in experimental samples, and explaining the reported disordered structures (Schorr 2007). Similarly to chalcopyrites CIGS, quaternary kesterite and stannite CZTS are obtained from the zincblende structure by replacing the Zn cations in such a way that each anion (Se or S) is coordinated by one Zn, one Sn and two Cu atoms. The existence of three distinct cations results in three different cation-anion bond lengths, which induce a displacement of the anion from its ideal zincblende site. That distortion is measured by the anion displacement parameters (u_x , u_y , u_z), i.e., the relative coordinates of the anion in the conventional body-centered tetragonal cell. The dispersion of experimental data for u is known to be large in CIGS compounds (Jaffe and Zunger 1984; Merino et al. 1996). Concerning CZTS, fewer structural measurements can be found in literature and in most cases only a and c are reported (Babu et al. 2008; Hahn and Schulze 1965; Hall et al. 1978; Olekseyuk et al. 2002; Schorr et al. 2007). Concerning the measured band gaps (Ahn et al. 2010; Kamoun et al. 2007; Katagiri et al. 2001; Nakayama and Ito 1996; Seol et al. 2003; Tanaka et al. 2005; Zhang et al. 2006), early studies suggested a value of about 1.4–1.6 eV both for S and Se compounds. This was in disagreement with density functional theory (DFT) calculations (Chen et al. 2009a; Persson 2010), using semi-local or hybrid functionals, which obtained systematically a smaller gap for Se compounds. More recent measurements (Ahn et al. 2010) delineate a gap of about 1 eV for $\text{Cu}_2\text{ZnSnSe}_4$, explaining the previous overestimation with the presence of ZnSe in the sample.

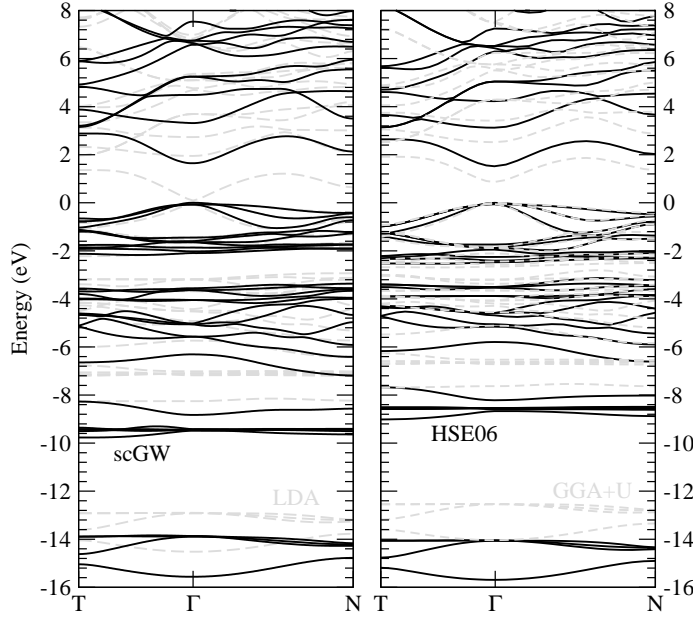


Figure 1.7 Band structures for kesterite $\text{Cu}_2\text{ZnSnS}_4$ calculated using: (left panel) DFT-LDA (dashed line) and *scGW* (continuous line), (right panel) GGA+*U* (dashed line) and HSE06 (continuous line). Top valence bands are set to zero. From Botti et al. (2011)

In Fig. 1.7, taken from Botti et al. (2011), we display band structures for kesterite $\text{Cu}_2\text{ZnSnS}_4$, obtained using different theoretical schemes at the experimental geometry. In the left panel, the KS LDA band structure is compared with the *scGW* bands. We observe that *scGW* corrections upshift almost rigidly the lowest conduction states. Concerning the valence: (i) the dispersion of the S *p*-Cu *d* antibonding states at the top of the valence remains fairly unaltered, even if the overlap of LDA and quasiparticle wavefunctions shows remarkable variations in this region. (ii) The band width of the S *p*-Cu *d* bonding states (located between -3.5 and -6.7 eV) slightly increases. (iii) The bands associated to the (Zn,Sn)-S bond (between -8 and -10 eV) are inverted and downshifted by about 2 eV with respect to LDA. (iv) Also the S *s* states are moved down by about 2 eV. In the right panel of Fig. 1.7 we show the same bands as obtained from GGA+*U* and HSE06 calculations. In this case HSE06 bands are remarkably similar to *scGW* bands. This is not particularly surprising as the Hartree-Fock mixing of HSE06 is particularly suited for materials with gaps of about 1–2 eV (Marques et al. 2011; Paier et al. 2008). As expected, GGA+*U* shifts down the states with Cu *d* character, thereby opening the gap to a reasonable value. However, it is evident from the figure, that the overall description of the band dispersions is quite inaccurate. Note that the analysis of the band structure of a CIGS compound or another CZTS compound would have lead to the same conclusions (Aguilera et al. 2011; Botti et al. 2011).

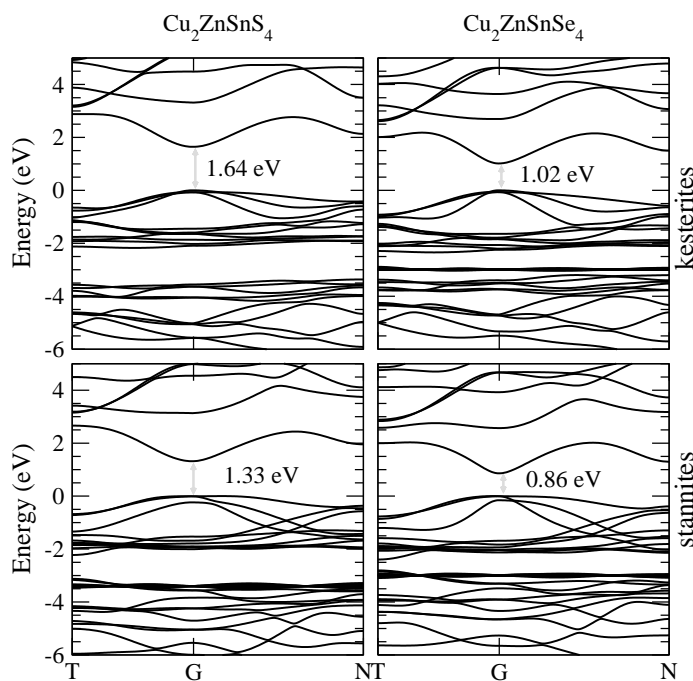


Figure 1.8 Band structures from *scGW* for (a) kesterite $\text{Cu}_2\text{ZnSnS}_4$, (b) stannite $\text{Cu}_2\text{ZnSnS}_4$, (c) kesterite $\text{Cu}_2\text{ZnSnSe}_4$, (d) stannite $\text{Cu}_2\text{ZnSnSe}_4$. From Botti et al. (2011)

In Fig. 1.8 we can see the *scGW* band structures of the four compounds of the CZTS family in the energy region close to the fundamental gap. For the kesterite $\text{Cu}_2\text{ZnSnS}_4$ and stannite $\text{Cu}_2\text{ZnSnSe}_4$ the experimental geometries were used (Babu et al. 2008; Hahn and Schulze 1965; Hall et al. 1978; Olekseyuk et al. 2002; Schorr et al. 2007). For the remaining compounds, the experimental anion displacements were not reported (Babu et al. 2008; Hahn and Schulze 1965; Hall et al. 1978; Olekseyuk et al. 2002; Schorr et al. 2007), and it was therefore necessary to resort to the theoretical structures.

The choice of the theoretical framework for the geometry optimization is essential. In fact, the strong dependence of the gap on anion displacements is also present in CZTS compounds (Botti et al. 2011). Also in this case slopes are substantially larger for *scGW* calculations than for DFT-LDA, and even than for HSE06. Once again, they are controlled by the screening, which is essential to include in a self-consistent way, as it is done in a *scGW* scheme. (Botti et al. 2011) verified that LDA/GGA relaxed structures lead to unacceptably large errors (up to 40%) in the *scGW* band gap, essentially related to the error in u : Cu-(S,Se) and Zn-(S,Se) bond lengths are too small in DFT-LDA, while Sn-(S,Se) bond lengths are too large. Also this time the solution to this issue relies on the use of the HSE06 functional, that yields extremely accurate values for u and the cell parameters, thanks to a better description of the localized states participating in

bonding.

The major difference among the four band structures of Fig. 1.8 is the width of the band gaps, which are in excellent agreement with experimental results. As in the CIGS family, Se compounds have a smaller gap with respect to S compounds. Furthermore, stannites have consistently smaller gaps than kesterites.

In conclusion, remarkable similarities were found in the electronic properties of stannites and kesterite CZTS, and, to a large extent, between CZTS and CIGS compounds. This fact suggests once more that CZTS materials are excellent candidates to replace more costly CIGS in the absorbing layer of thin film photovoltaic devices.

We want to conclude this section with an example of optical spectra calculated from *scGW* band structures, which is reported in Aguilera et al. (2011).

Starting either from the KS and *scGW* band structures of CuGaS₂, Aguilera et al. (2011) calculated optical absorption spectra within linear response, both applying TDDFT and solving the Bethe-Salpeter equation (BSE). Figs 1.9 and 1.10 from Aguilera et al. (2011) show calculations of the imaginary part of the macroscopic dielectric function for light polarized along the *c*-axis. The theoretical curves are also compared with the experimental data published in Levchenko et al. (2007) and Rife et al. (1977).

The experimental dielectric functions of Alonso et al. (2001) were obtained with ellipsometry at room temperature, whereas the spectra of Levchenko et al. (2007) were extracted from reflection spectra measured at 77 K, using the Kramers-Kronig relations. Both results are for single-crystal samples. We can observe that the two curves are rather different. In particular, the absorption spectrum of Levchenko et al. (2007) has a much smaller intensity (around the half) than the experimental curve of Alonso et al. (2001) and previous results by Rife et al. (1977), probably due to the quality of the reflecting surface of the samples. In view of the above, the intensity of the absorption spectrum of Levchenko et al. (2007) was rescaled. Another discrepancy among the available experimental data concerns the behavior of the spectra at around 5 eV. While the measurements of Alonso et al. (2001) found a plateau in the absorption after the peak at 4 eV, in Levchenko et al. (2007) and Rife et al. (1977) a deep valley appears after 4 eV. Note that there are substantial discrepancies between the two experiments and that sufficiently accurate *ab initio* calculations are an essential tool to discriminate between the two sets of data.

In Fig. 1.9 we compare results obtained within the RPA using *scCOHSEX*+ G_0W_0 eigenvalues, and ALDA using KS eigenvalues. The RPA curve obtained using KS eigenvalues overlaps almost perfectly with the ALDA curve. This proves that the inclusion of the ALDA kernel does not have any relevant effect on the absorption, as the important contributions due to electron-electron and electron-hole interactions are not accounted for by the ALDA kernel (Botti et al. 2004; Gavrilenko and Bechstedt 1997; Onida et al. 2002). Both the RPA and ALDA spectra using KS-GGA eigenvalues are dramatically red-shifted. As a first conclusion, we can observe that the accuracy of RPA or ALDA *ab initio* calculations alone would not be sufficient to explain the large discrepancies among experimental optical measurements.

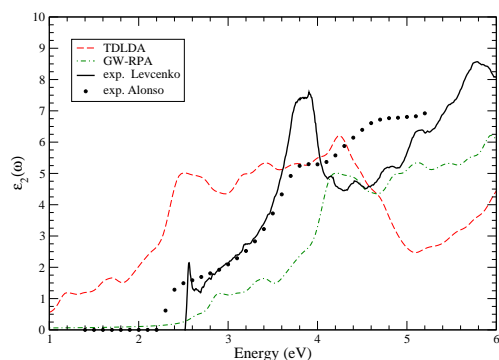


Figure 1.9 (Color online) Imaginary part of the dielectric function for light polarized along the *c*-axis obtained with: TDDFT using the ALDA kernel (dashed line), RPA using *GW* eigenvalues (dot-dashed line) compared to experimental data of Alonso et al. (2001) (dots) and Levchenko et al. (2007) (solid line; in arb. units, see text). From Aguilera et al. (2011)

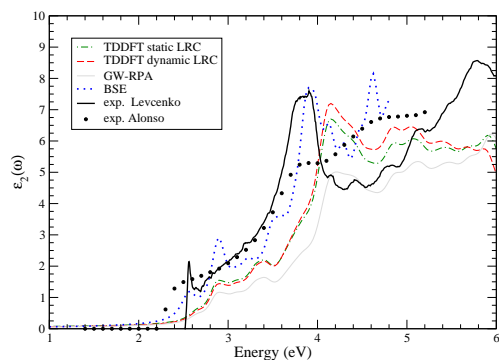


Figure 1.10 (Color online) Imaginary part of the dielectric function for light polarized along the *c*-axis obtained with: TDDFT using the static (dot-dashed line) and the dynamic (dashed line) LRC kernel, GW-RPA (gray solid line) and BSE (dotted line), compared to experimental measurements of Alonso et al. (2001) (larger dots) and Levchenko et al. (2007) (solid line; in arb. units). From Aguilera et al. (2011)

If the $\text{scCOHSEX}+G_0W_0$ eigenvalues are used for a RPA calculation (dot-dashed line), the resulting spectra are blue-shifted, while the line shape does not change. As a result, the absorption peaks are now at too high energies. In fact, in the energy range of interest for absorption the *GW* correction is basically equivalent to applying a scissor operator.

What is still missing is a proper account of excitonic effects. For many intermediate-gap semiconductors, it was shown (Botti et al. 2005, 2004;

Reining et al. 2002) that the long-range contribution (LRC) to the exchange-correlation kernel was enough to yield a good agreement with experimental absorption spectra. The LRC kernel works particularly well in the case of a continuum exciton, giving in general very good optical properties with the efficiency of a TDDFT calculation. In Fig. 1.10 we show the spectra obtained using the static (Botti et al. 2004; Reining et al. 2002) and the dynamic (Botti et al. 2005) versions of the LRC kernel. $scCOHSEX+G_0W_0$ eigenvalues were used in these calculations.

The TDDFT-LRC spectra shown in Fig. 1.10 provide a clear improvement with respect to the curves displayed in Fig. 1.9. The intensity of the peaks as well as the onsets of absorption are now closer to experiment. However, the peak at about 4 eV is still located at a higher energy than its experimental position. Note that the excitonic peak at the fundamental edge in $CuGaS_2$ has the nature of a bound exciton, even if the binding energy is rather small. This explains why the LRC models do not reproduce perfectly the BSE result.

If one wants a precise description of the bound excitonic peak of $CuGaS_2$ (Bellabarba et al. 1996; Levchenko et al. 2007; Ringeissen et al. 1973; Tell and Kasper 1973) it is necessary to resort to the solution of the BSE. In Fig. 1.10 we see that, in spite of the fact that a shifted mesh of 1000 \mathbf{k} -points is not sufficiently dense to smooth out the curve due to the strong dispersion of the lowest conduction state, the experimental onset (at about 2.55 eV) and the peak at about 3.8 eV are well reproduced in the BSE calculation (Aguilera et al. 2011). At the absorption edge, the estimate of the excitonic binding energy of about 0.1 eV is also consistent with experimental data (Syrbu et al. 2005).

However, one cannot not forget that TDDFT calculations using model exchange-correlation kernels are much less involved than the solution of the BSE. In many cases, for example when dealing with supercells with defects or doping, the only feasible approach that guarantees qualitatively correct results is to perform TDDFT calculations using model kernels derived from Bethe-Salpeter.

1.3.2 *Delafossite transparent conductive oxides*

Transparent conductive oxides (TCOs) are wide bandgap semiconductors characterized by large free carrier densities. These carriers are created by either intrinsic or extrinsic doping, giving to TCOs both low resistivity and transparency in the visible energy window. The most common examples of TCOs are n-doped semiconductors such as SnO_2 , In_2O_3 , and ZnO . Carrier concentrations up to 10^{21} cm^{-3} are commonly achieved with large mobilities of $30 \text{ cm}^2/\text{Vs}$, giving rise to conductivities of up to 3000 S/cm (Ginley 2010). Up to now p-type conductivity has been much harder to achieve. The reason is related to well-known differences between holes and electrons in TCOs. First, holes have a much heavier mass than electrons and consequently much lower mobility. Second, doping rules point to the difficulty of p-type doping in oxides (Zunger 2003) because of the high electronegativity and the presence of hole killers, such as V_O , with relatively low formation energy.

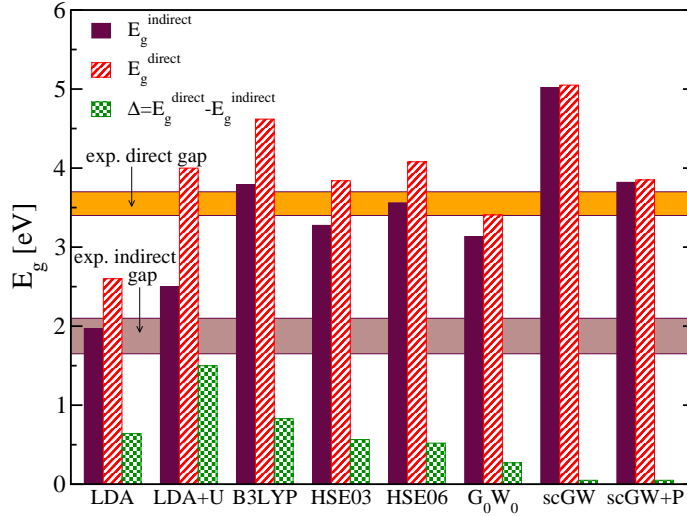


Figure 1.11 Band gaps of CuAlO_2 using: LDA, LDA+ U , hybrid, G_0W_0 , scGW, and scGW including model polaronic corrections. The horizontal zones contain data extracted from various optical experiments. From Vidal et al. (2010b)

Nevertheless, p-type conductivity was found in delafossite CuAlO_2 thin films (Kawazoe et al. 1997). Few years later, bipolar (both n- and p-type) conductivity was discovered in CuInO_2 (Nie et al. 2002; Yanagi et al. 2001), another element of the same delafossite family. However, in p-type TCOs carrier concentrations remain smaller than 10^{18} cm^{-3} and mobilities limited to $\mu < 1 \text{ cm}^2/\text{Vs}$, resulting in conductivities of 100 S/cm (Ginley 2010). Other p-type oxides belonging to different families were found afterwards, namely ZnRh_2O_4 (Mizoguchi et al. 2002) and SnO (Ogo et al. 2008). Even though they have relatively low absorption onsets (at 2.1 eV and 2.9 eV, respectively) and, consequently, they can hardly be considered transparent, they display significantly higher p-type conductivity than delafossites. These spectacular findings opened the way for the fabrication of TCO p-n junctions (Yanagi et al. 2002), and to the development of a new technology entirely based on “invisible circuits” (Banerjee et al. 2005; Ohta et al. 2003; Thomas 1997). Many innovative applications require transparent electronics, such as stacked solar cells, transparent screens, or functional windows that generate solar electricity.

CuAlO_2 is by far the most studied system of the family of delafossite TCOs, both theoretically and experimentally. For a long time, there has been no agreement neither on the origin of the p-type conductivity, nor on the electronic band gap of the pure crystal. Measurements of the direct *optical* band gap (E_g^{dir}) of CuAlO_2 fall in the range from 2.9 to 3.9 eV (Alkoy and Kelly 2005; Banerjee and Chattopadhyay 2005; Banerjee et al. 2005, 2003, 2004; Benko and Koffyberg 1984; Dittrich et al. 2004; Gilliland et al. 2007; Kawazoe et al. 1997; Ong and Gong 2003; Pellicer-Porres et al. 2006; Tate et al.

2009; Yanagi et al. 2000; Yu et al. 2007), with most values in the interval 3.4–3.7 eV. These experiments also yield a large dispersion of indirect gaps (E_g^{ind}), from 1.65 to 2.1 eV, with one experiment measuring 2.99 eV (Pellicer-Porres et al. 2006). Unfortunately, there is only one photoemission experiment (Yanagi et al. 2000) that gives a value of 3.5 eV for the *quasiparticle* band gap. Note that the *optical* and *quasiparticle* gaps differ by the exciton binding energy. Concerning CuInO_2 , optical experiments measured E_g^{dir} between 3.9 and 4.45 eV (Sasaki and Shimode 2003; Teplin et al. 2004; Yanagi et al. 2001), with only one estimation of E_g^{ind} at 1.44 eV (Sasaki and Shimode 2003).

From the theoretical perspective, the situation is also quite complex, even if the full Cu *3d* shell should exclude the strongly correlated electron regime. These materials are usually studied in literature within DFT, using the standard LDA or GGA (Gilliland et al. 2007; Ingram et al. 2001; Nie et al. 2002; Pellicer-Porres et al. 2006; Robertson et al. 2002; Shi et al. 2008; Yanagi et al. 2000). We can expect that the Kohn-Sham band structures yield underestimated band gaps and the hybridization between the *d* electrons of the metal and *p* electrons of oxygen is misrepresented (Bruneval et al. 2006b; Vidal et al. 2010a).

Both LDA/GGA+*U* and hybrid functionals have been applied to study members of the delafossite family with some success (Huda et al. 2009; Laskowski et al. 2009; Robertson et al. 2002; Trani et al. 2010; Vidal et al. 2010b). Note that these calculations yield quasiparticle gaps, and not optical gaps. To evaluate these latter quantities one mostly resorts to the solution of the Bethe-Salpeter equation. For delafossite structures there is one such calculation starting from a GGA+*U* band structure (Laskowski et al. 2009). It yields for CuAlO_2 a very large exciton binding energy of about 0.5 eV for the first direct transition. The choice of the parameter *U* was found to have significant consequences on the width of the band gap, but it did not affect significantly the exciton binding energy. We can thus assume that 0.5 eV is a reasonable estimate of this latter quantity.

In the following, we discuss calculations from Trani et al. (2010); Vidal et al. (2010b) of the band structures of CuAlO_2 and CuInO_2 , comparing the most accurate theoretical tools available in the community. These include standard LDA, hybrid functionals (namely B3LYP (Stephens et al. 1994) and two flavors of Heyd-Scuseria-Ernzerhof, HSE03 and HSE06 (Heyd et al. 2003, 2006)), LDA+*U*, G_0W_0 and *scGW*. We expect *scGW* to be the most accurate *ab initio* approach.

In Fig. 1.11 we show a summary of calculated direct and indirect photoemission gaps of CuAlO_2 from Vidal et al. (2010b). The corresponding band structures are shown in Fig. 1.12. The minimum E_g^{dir} of CuAlO_2 is always found at L, where the dipole transition between the band edge states is allowed (Nie et al. 2002). All calculations, except *scGW*, give a fundamental E_g^{ind} between the conduction band minimum at Γ and the valence band maximum along the Γ -F line. The experimental data for optical gaps are also presented with an error bar that reflects the dispersion of the most likely values found in literature. LDA exhibits, as expected, the smallest gaps. Basically every approach beyond it opens up the gap by different amounts and modifies the band dispersions. The direct and indirect gaps have

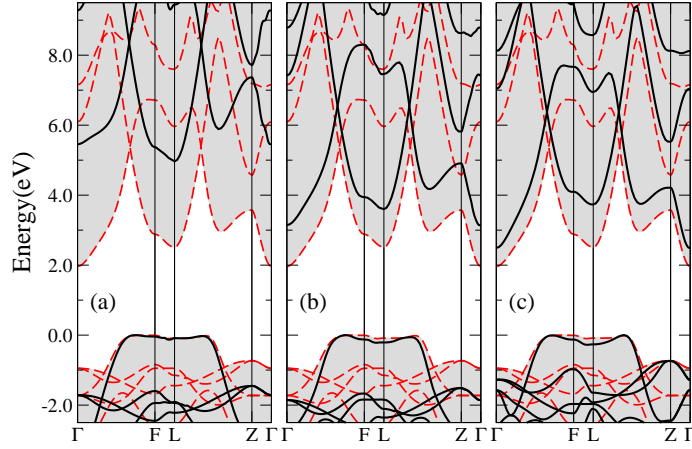


Figure 1.12 Band structures for CuAlO_2 : comparison of LDA (red dashed lines) with *scGW* (a), HSE03 (b), and LDA+*U* (c). From Vidal et al. (2010b)

similar behaviors in the different theories, and both increase when going from $\text{LDA} < G_0W_0 < \text{HSE03} < \text{HSE06} < \text{B3LYP} < \text{scGW}$.

Looking at the direct gap, we point out that most of the methods give results that are within the experimental range, when an exciton binding energy of around 0.5 eV (Laskowski et al. 2009) is considered. This is true for LDA+*U*, G_0W_0 , the hybrids HSE03 and HSE06. However, for *scGW* and even for B3LYP, the theoretical gap is larger by about 1–1.5 eV than the experimental findings.

We observe that the difference $E_g^{\text{dir}} - E_g^{\text{ind}}$ decreases with the sophistication of the method, reaching nearly zero for the *scGW* calculation. This is a consequence of the drastic change of the conduction band dispersion, which displaces the conduction minimum from Γ to L when *scGW* is applied (see Fig. 1.12). The lowest conduction bands cross along the line between the high-symmetry points L and F, which results in a significant change in the character of the conduction band minimum. At Γ and Z the band has a e_g Cu 3*d* character with a significant amount of *s* and *p* states from Al, O and Cu. On the other hand, at L and F, the bottom conduction bands is composed of Cu *s* and O *p* states. Therefore, it is not surprising that *GW* correction are so strongly \mathbf{k} -point dependent. Figure 1.13 displays the difference between expectation value of the Hartree potential and the exchange part of the self-energy, constructed with DFT wave functions or with *scCOHSEX* wave functions. The exchange self-energy changes up to 4 eV, while the Hartree term is rather constant. We note that often in semiconductor physics one assumes that the quasiparticle corrections can be modeled by a rigid shift (the so-called scissor operator). From these results it follows that one should refrain from using this simple approximation for delafossite TCOs.

Hybrid methods such as HSE03, HSE06 and B3LYP open the band gaps and reduce the difference $E_g^{\text{dir}} - E_g^{\text{ind}}$, following the trend observed for *scGW* calculations. The conduction band minimum (CBM) from HSE03 is still located

at Γ , but the difference between the CBM at L and Γ gets significantly smaller. The main effect of LDA+ U is to open the LDA gap by an amount that can be controlled by the parameter U . The difference $E_g^{\text{dir}} - E_g^{\text{ind}}$ is increased within the LDA+ U approximation, due to the change of character for the lowest conduction band along the symmetry line between Γ and F. We can conclude that hybrid calculations give a better description (i.e., closer to sc*GW*) of band dispersions than LDA+ U , even if the two approaches yield similar band gaps.

For CuInO₂ the smallest E_g^{dir} is located at Γ , where optical transitions are forbidden (Nie et al. 2002). A meaningful comparison with optical experiments must then consider the gap at L. Both trends and quantitative results are analogous to those for CuAlO₂. In particular, sc*GW* yields again E_g^{dir} larger by 1–1.5 eV than the experimental range (Trani et al. 2010; Vidal et al. 2010b).

We stress again that, to date, sc*GW* is arguably the best method available to estimate band gaps of wide-gap semiconductors, and that it gives excellent results for compounds like Cu₂O and CuIn(S,Se)₂ (Bruneval et al. 2006b; Vidal et al. 2010a). It is unlikely that the presence of defects can explain the discrepancy between experiments and sc*GW* gaps. However, there is another effect that has been neglected up to now: the change of screening due to the polarization of the lattice. The polaron constant defined as $\alpha_p = (1/\epsilon_\infty - 1/\epsilon_0)(\hbar/2ma_B^2\omega_{\text{LO}})^{1/2}$, where a_B is the Bohr radius, ω_{LO} the longitudinal optical frequency of the highest E_u phonon mode, ϵ_∞ and ϵ_0 the low frequency electronic and the static dielectric constants, respectively, measures the strength of the polaronic effect. According to the experimental data (Pellicer-Porres et al. 2009), unfortunately available only for CuAlO₂, the polaron constant for this system is large ($\alpha_p \sim 1$), indicating a non-negligible contribution of the lattice polarization to the electronic screening. It is known that in other ionic compounds with similar polaron constants this can lead to the shrinking of the band gap by about 1 eV (Bechstedt et al. 2005). A full sc*GW* calculation including, in an *ab initio* framework, the effects of the lattice polarization is still beyond reach. However, a reliable estimate was obtained using the model proposed by Bechstedt et al. (2005), which gives a static representation of the contribution of lattice polarization to the screening based on difference of experimental static dielectric constants. By performing a perturbative *GW* step, including a model contribution to the screening due to lattice polarization, on top of the scCOHSEX, Vidal et al. (2010b) found a uniform (k-independent) decrease of the band gap by 1.2 eV. As we can see in Fig. 1.11, this correction brings the sc*GW* results for E_g^{dir} well within the experimental range (once the excitonic correction of about 0.5 eV is also considered). As it is observed in Bechstedt et al. (2005), the model employed to account for the lattice polarization can only overestimate the correction. All these results point to the conclusion that the agreement of the other methods with experiment was fortuitous and due to a cancellation of errors.

It is interesting to notice that to design p-type TCOs it is recommended the use of layered structures in order to increase the value of the band gap. Indeed, LaCuSO (Ueda et al. 2000) and BaCu(S,Se,Te)F (Zakutayev et al. 2010) display band structures very similar to the one of CuAlO₂. One can foresee that

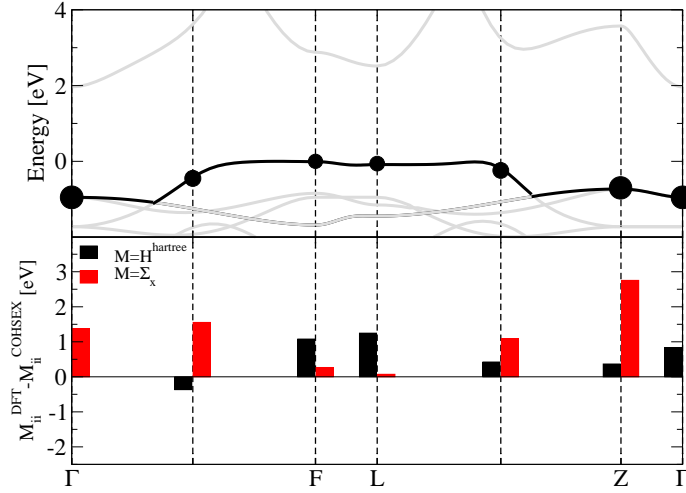


Figure 1.13 Top panel: Kohn-Sham conduction band structure of CuAlO₂. Bottom panels: difference between the expectation value of the operator M ($M = H^{Hartree}, \Sigma_x$) constructed with DFT wave functions or with scCOHSEX wave functions for the bottom conduction band. From Trani et al. (2010).

also in these materials the renormalization of the band gap due to the lattice contribution to the screening could then play an important role and significantly affect the interpretation of experiments.

To conclude, we focus now on the indirect gaps of Fig. 1.11. Analogous conclusions could be obtained for CuInO₂ or CuGaO₂ Trani et al. (2010); Vidal et al. (2010b), but we rather focus on CuAlO₂ as more experimental data are available in literature. All hybrids and *GW* calculations yield indirect gaps much larger than the experimental range 1.65–2.1 eV, even taking into account any possible excitonic and polaronic effects. Moreover, sc*GW*, the best method used in this work, yields the highest E_g^{ind} at around 5 eV, while the difference $E_g^{dir} - E_g^{ind}$ is in general much smaller than the experimental value (≈ 2 eV), and even vanishing for sc*GW* calculations.

These are very strong arguments in favor of Robertson et al. (2002) that suggested that the experimental “indirect gap” absorption was due to defects, and should not be present in the defect-free compound. Also Pellicer-Porres et al. (2006) questioned the interpretation of the low energy peaks as indirect transitions, as the absorption coefficient is more than two orders of magnitude larger than in typical indirect absorption edges. It has been first asserted that the defects that could be responsible are oxygen interstitials O_i, as DFT calculations within the LDA predict low formation energies and the introduction of states in the gap at 0.7 and 1.4 eV (Hamada and Katayama-Yoshida 2006). More recently, Scanlon and Watson (n.d.) proposed, based on screened hybrid calculations, that antisite Cu-on-Al Cu_{Al} is responsible for the features in the absorption spectra at 1.65-2.1 eV.

In summary, it is clear that the compounds of the delafossite family exhibit complex and unusual band gap physics that can not be captured by standard theoretical approximations. In particular, the direct band gap is well reproduced by the state-of-the-art many-body approaches if the contribution of lattice polarization to the screening is taken into account. We can expect that this situation, of a large gap that is reduced substantially by polaronic effects, is quite general and is present in many polar materials. In fact, the apparent good agreement between calculated gaps (with hybrid functionals or G_0W_0) and experimental gaps for materials as simple and widely studied as LiF can be accidental: the underestimation of the gap by these methods (the *scGW* gap is indeed 2 eV larger than the experimental and G_0W_0 gap) is compensated by the neglect of lattice polarization effects. Furthermore, the modifications with respect to the LDA Kohn-Sham bands are strongly k -dependent, which makes questionable the common practice of using a scissor operator. The band dispersion obtained by hybrid functional calculations is in between the LDA and *scGW* dispersion, while the LDA+ U calculations open up the gap but do not give a significant improvement of the band dispersion. This is in agreement with what we have discussed in Sec. 1.3.1 for CIGS and CZTS compounds. Finally, *scGW* calculations rule out the interpretation of the low energy features in the absorption spectra as arising from a putative indirect band gap. These structures should rather come from intrinsic defects, as proposed in Refs. (Pellicer-Porres et al. 2006; Robertson et al. 2002). However, a complete understanding of the electronic and excitation properties of these systems will only be achieved, in our opinion, by a high-level theoretical scheme (such as *scGW*) including defects and effects from the lattice polarization in an *ab initio* framework.

1.4 Conclusions

The response upon excitation of complex materials, such as materials for thin-film photovoltaics, can nowadays be calculated from first-principles with high accuracy. This was made possible by recent theoretical developments together with the optimization of computer codes.

When dealing with electronic excitations, the knowledge of the ground state density of the system is no longer sufficient, which means that one has to find appropriate ways to go beyond density functional theory. Different paths have been explored for the past years, based on Green's functions, the time-dependent density, hybrid functionals in the generalized Kohn-Sham picture, and empirically modified Hamiltonians.

The state-of-the-art approach to calculate band structures and optical spectra, quantitatively comparable to experimental data, relies on the many-body perturbation theory via the *GW* approximation and the solution of the Bethe-Salpeter equation. However, one has to deal with one-particle and two-particle Green's functions, that require heavy calculations to be determined.

The *GW* approximation for the calculation of quasiparticle states, either in the perturbative or in the self-consistent schemes, cannot be applied at the moment

to materials including d electrons if the unit cell is larger than 20–30 atoms.

As long as large supercells are out of reach for *GW* calculations, hybrid functionals promise to be a computationally efficient alternative with a satisfactory degree of accuracy. This fact motivates the search for improved approximations for the mixing parameter of hybrid functionals, that include screening as a physical ingredient.

In a similar way, whenever the solution of the Bethe-Salpeter equation is out of reach to determine absorption spectra, one can obtain qualitatively reliable results by performing time-dependent density functional theory calculations, by applying model kernels derived from Bethe-Salpeter.

The way is open now for many possible applications. Indeed, in the rapidly expanding field of photovoltaics, the understanding of many problems of great complexity and technological interest is still lacking, especially concerning defects and interfaces. Even if great physical insight can already be obtained employing existing methods, the quest for improved approximations, as well as the search for novel theoretical approaches, cannot be abandoned. Hopefully new developments will appear in the next years.

References

- Abrahams SC and Bernstein JL 1973 Piezoelectric nonlinear optic CuGaS_2 and CuInS_2 crystal structure: Sublattice distortion in A1B3 and A2B4 type chalcopyrites. *J. Chem. Phys.* **59**, 5415–5422.
- Adragna G, Del Sole R and Marini A 2003 *Ab initio* calculation of the exchange-correlation kernel in extended systems. *Phys. Rev. B* **68**, 165108.
- Aguilera I, Vidal J, Wahnón P, Reining L and Botti S 2011 First-principles study of the band structure and optical absorption of CuGaS_2 . *Phys. Rev. B* **84**, 085145.
- Ahn S, Jung S, Gwak J, Cho A, Shin K, Yoon K, Park D, Cheong H and Yun JH 2010 Determination of band gap energy of $\text{Cu}_2\text{ZnSnSe}_4$ thin films: On the discrepancies of reported band gap values. *Appl. Phys. Lett.* **97**, 021905.
- Alkauskas A, Broqvist P and Pasquarello A 2010 Defect levels through hybrid density functionals: Insights and applications. *Phys. Status Solidi B* **248**, 775.
- Alkoy E and Kelly P 2005 The structure and properties of copper oxide and copper aluminium oxide coatings prepared by pulsed magnetron sputtering of powder targets. *Vacuum* **79**, 221–230.
- Alonso MI, Wakita K, Pascual J, Garriga M and Yamamoto N 2001 Optical functions and electronic structure of CuInSe_2 , CuGaSe_2 , CuInS_2 , and CuGaS_2 . *Phys. Rev. B* **63**, 075203.
- Anisimov VI, Zaanen J and Andersen OK 1991. *Phys. Rev. B* **44**, 943.
- Aulbur WG, L. Jönsson and Wilkins JW 1999. *Solid State Physics* **54**, 1.
- Babu G, Kumar Y, Bhaskar P and Raja V 2008 Effect of post-deposition annealing on the growth of $\text{Cu}_2\text{ZnSnSe}_4$ thin films for a solar cell absorber layer. *Semicond. Sci. Technol.* **23**, 085023.
- Banerjee A and Chattopadhyay K 2005 Size-dependent optical properties of sputter-deposited nanocrystalline p-type transparent CuAlO_2 thin films. *J. Appl. Phys.* **97**, 084308.
- Banerjee A, Ghosh C, Das S and Chattopadhyay K 2005 Electro-optical characteristics and field-emission properties of reactive dc-sputtered p- CuAlO_{2+x} thin films. *Physica B* **370**, 264–276.
- Banerjee A, Kundoo S and Chattopadhyay K 2003 Synthesis and characterization of p-type transparent conducting CuAlO_2 thin film by dc sputtering. *Thin Solid Films* **440**, 5–10.
- Banerjee A, Maity R and Chattopadhyay K 2004 Preparation of p-type transparent conducting CuAlO_2 thin films by reactive dc sputtering. *Mat. Lett.* **58**, 10–13.
- Bechstedt F, Seino K, Hahn PH and Schmidt WG 2005 Quasiparticle bands and optical spectra of highly ionic crystals: AlN and NaCl. *Phys. Rev. B* **72**, 245114.
- Bellabarba C, González J and Rincón C 1996 Optical-absorption spectrum near the exciton band edge in CuGaS_2 at 5 K. *Phys. Rev. B* **53**, 7792–7796.
- Benko F and Koffyberg F 1984 Opto-electronic properties of CuAlO_2 . *J. Phys. Chem. Solids* **45**, 57–59.
- Bloch PE 1994 Projector augmented-wave method. *Phys. Rev. B* **50**, 17953–17979.

- Botti S, Fourreau A, Nguyen F, Renault YO, Sottile F and Reining L 2005 Energy dependence of the exchange-correlation kernel of time-dependent density functional theory: A simple model for solids. *Phys. Rev. B* **72**, 125203.
- Botti S, Kammerlander D and Marques MAL 2011. *Appl. Phys. Lett.* **98**, 241915.
- Botti S, Schindlmayr A, Del Sole R and Reining L 2007 Time-dependent density functional theory for extended systems. *Rep. Prog. Phys.* **70**, 357.
- Botti S, Sottile F, Vast N, Olevano V, Reining L, Weissker HC, Rubio A, Onida G, Del Sole R and Godby RW 2004 Long-range contribution to the exchange-correlation kernel of time-dependent density functional theory. *Phys. Rev. B* **69**, 155112.
- Brothers EN, Izmaylov AF, Normand JO, Barone V and Scuseria GE 2008 Accurate solid-state band gaps via screened hybrid electronic structure calculations. *J. Chem. Phys.* **129**, 011102.
- Bruneval F, Vast N and Reining L 2006a Effect of self-consistency on quasiparticles in solids. *Phys. Rev. B* **74**, 045102.
- Bruneval F, Vast N, Reining L, Izquierdo M, Sirotti F and Barrett N 2006b Exchange and correlation effects in electronic excitations of Cu_2O . *Phys. Rev. Lett.* **97**, 267601.
- Bylander DM and Kleinman L 1990 Good semiconductor band gaps with a modified local-density approximation. *Phys. Rev. B* **41**, 7868–7871.
- Chapin D, Fuller C and Pearson G 2004 A new silicon p-n junction photocell for converting solar radiation into electrical power. *J. Appl. Phys.* **25**, 676.
- Chen S, Gong XG, Walsh A and Wei SH 2009a Crystal and electronic band structure of $\text{Cu}_2\text{ZnSnX}_4$ ($X = \text{S}$ and Se) photovoltaic absorbers: First-principles insights. *Appl. Phys. Lett.* **94**, 041903.
- Chen S, Gong XG, Walsh A and Wei SH 2009b Electronic structure and stability of quaternary chalcogenide semiconductors derived from cation cross-substitution of II-VI and I-III-VI₂ compounds. *Phys. Rev. B* **79**, 165211.
- Chen S, Gong XG, Walsh A and Wei SH 2010a Defect physics of the kesterite thin-film solar cell absorber $\text{Cu}_2\text{ZnSnS}_4$. *Appl. Phys. Lett.* **96**, 021902.
- Chen S, Walsh A, Luo Y, Yang JH, Gong XG and Wei SH 2010b Wurtzite-derived polytypes of kesterite and stannite quaternary chalcogenide semiconductors. *Phys. Rev. B* **82**, 195203.
- Clark S and Robertson J 2010 Screened exchange density functional applied to solids. *Phys. Rev. B* **82**, 085208.
- Del Sole R, Reining L and Godby RW 1994 $\text{Gw}\Gamma$ approximation for electron self-energies in semiconductors and insulators. *Phys. Rev. B* **49**, 8024–8028.
- Dittrich T, Dloczik L, Guminskaya T, Lux-Steiner M, Grigorieva N and Urban I 2004 Photovoltage characterization of CuAlO_2 crystallites. *Appl. Phys. Lett.* **85**, 742–744.
- Domain C, Laribia S, Tauniera S and Guillemoles JF 2003 Ab initio calculation of intrinsic point defects in CuInSe_2 . *J. Phys. Chem. Solids* **64**, 1657–1663.
- Ernzerhof M and Scuseria GE 1999 Assessment of the Perdew-Burke-Ernzerhof exchange-correlation functional. *J. Chem. Phys.* **110**, 5029.
- Faleev SV, van Schilfgaarde M and Kotani T 2004 All-electron self-consistent GW approximation: Application to Si, MnO, and NiO. *Phys. Rev. Lett.* **93**, 126406.
- Fetter AL and Walecka JD 1971 *Quantum Theory of Many-Particle Systems*. McGraw-Hill, New York.
- Fuchs F and Bechstedt F 2008 Indium-oxide polymorphs from first principles: Quasiparticle electronic states. *Phys. Rev. B* **77**, 155107.
- Gatti M, Bruneval F, Olevano V and Reining L 2007 Understanding correlations in vanadium dioxide from first principles. *Phys. Rev. Lett.* **99**, 266402.
- Gavrilenko VI and Bechstedt F 1997 Optical functions of semiconductors beyond density-functional theory and random-phase approximation. *Phys. Rev. B* **55**, 4343–4352.
- Gilliland S, Pellicer-Porres J, Segura A, Munoz A, Rodriguez-Hernandez P, Kim D, Lee MS and Kim TY 2007 Electronic structure of CuAlO_2 and CuScO_2 delafossites under pressure. *Phys. Stat. Sol. (b)* **244**, 309–314.
- Ginley D 2010 *Handbook of Transparent Conductors*. Springer Verlag.
- Godby RW, Schlüter M and Sham LJ 1987 Trends in self-energy operators and their corresponding exchange-correlation potentials. *Phys. Rev. B* **36**, 6497–6500.
- Godby RW, Schlüter M and Sham LJ 1988 Self-energy operators and exchange-correlation potentials in semiconductors. *Phys. Rev. B* **37**, 10159–10175.
- Gonze X, Ghosez P and Godby RW 1995 Density-polarization functional theory of the response of a periodic insulating solid to an electric field. *Phys. Rev. Lett.* **74**, 4035–4038.
- Gonze X, Rignanese GM, Verstraete M, Beuken JM, Pouillon Y, Caracas R, Jollet F, Torrent M, Zerah G, Mikami M, Ghosez P, Veithen M, Raty JY, Olevano V, Bruneval F, Reining L, Godby R, Onida G, Hamann D and Allan D 2005 A brief introduction to the ABINIT software package. *Z. Kristallogr.* **220**, 558–562.
- Green M 2000 *Power to the people: sunlight to electricity using solar cells*. Univ of New South Wales.

- Gross EKV and Kohn W 1985 Local density-functional theory of frequency-dependent linear response. *Phys. Rev. Lett.* **55**, 2850–2852.
- Gross EKV and Kohn W 1986 Local density-functional theory of frequency-dependent linear response. *Phys. Rev. Lett.* **57**, 923–923(E).
- Gross EKV, Dobson FJ and Petersilka M 1996 *Topics in Current Chemistry* vol. 181 Nalewajski, R. F. edn Springer-Verlag Heidelberg p. 81.
- Guillemoles JF, Kronik L, Cahen D, Rau U, Jasenek A and Schock HW 2000 Stability issues of Cu(In, Ga)Se₂-based solar cells. *J. Phys. Chem. B* **104**, 4849–4862.
- Gygi F and Baldereschi A 1989 Quasiparticle energies in semiconductors: Self-energy correction to the local-density approximation. *Phys. Rev. Lett.* **62**, 2160–2163.
- Hahn H and Schulze H 1965. *Naturwiss.* **52**, 426.
- Hall S, Szymanski J and Stewart J 1978 Kesterite Cu₂(Zn,Fe)SnS₄ and stannite Cu₂(Fe,Zn)SnS₄ structurally similar but distinct minerals. *Can. Mineral.* **16**, 131.
- Hamada I and Katayama-Yoshida H 2006 Energetics of native defects in CuAlO₂. *Physica B* **376–377**, 808–811.
- Hanke W 1978 Dielectric theory of elementary excitations in crystals. *Adv. Phys.* **27**, 287–341.
- Hedin L 1965 New Method for Calculating the One-Particle Green's Function with Application to the Electron-Gas Problem. *Phys. Rev.* **139**, A796.
- Heyd J, Scuseria GE and Ernzerhof M 2003 Hybrid functionals based on a screened coulomb potential. *J. Chem. Phys.* **118**, 8207.
- Heyd J, Scuseria GE and Ernzerhof M 2006 Erratum: Hybrid functionals based on a screened coulomb potential. *J. Chem. Phys.* **124**, 219906(E).
- Hohenberg P and Kohn W 1964 Inhomogeneous electron gas. *Phys. Rev.* **136**, B864–B871.
- Huda MN, Yan Y, Walsh A, Wei SH and Al-Jassim MM 2009 Group-III A versus III B delafossites: Electronic structure study. *Phys. Rev. B* **80**, 035205.
- Hybertsen MS and Louie SG 1985 First-principles theory of quasiparticles: Calculation of band gaps in semiconductors and insulators. *Phys. Rev. Lett.* **55**, 1418–1421.
- Hybertsen MS and Louie SG 1986 Electron correlation in semiconductors and insulators: Band gaps and quasiparticle energies. *Phys. Rev. B* **34**, 5390–5413.
- Ingram BJ, Mason TO, Asahi R, Park KT and Freeman AJ 2001 Electronic structure and small polaron hole transport of copper aluminate. *Phys. Rev. B* **64**, 155114.
- Jackson P, Hariskos D, Lotter E, Paetel S, Wuerz R, Menner R, Wischmann W and Powalla M 2011 New world record efficiency for Cu(In,Ga)Se₂ thin-film solar cells beyond 20%. *Prog. Photovolt: Res. Appl.*
- Jaffe JE and Zunger A 1983 Anion displacement and band gap anomaly in ternary ABC₂ chalcopyrite semiconductors. *Phys. Rev. B* **27**, 5176.
- Jaffe JE and Zunger A 1984 Theory of the band-gap anomaly in ABC₂ chalcopyrite semiconductors. *Phys. Rev. B* **29**, 1882.
- Jiang FD and Feng JY 2008 Electronic modification of Cu-based chalcopyrite semiconductors induced by lattice deformation and composition alchemy. *Semicond. Sci. Technol.* **23**, 025001.
- Jiang H, Gomez-Abal RI, Rinke P and Scheffler M 2009 Localized and itinerant states in lanthanide oxides united by GWLDA+U. *Phys. Rev. Lett.* **102**, 126403.
- Kammerlander D, Marques M and Botti S 2011 Band structures of Cu₂ZnSnS₄ and Cu₂ZnSnSe₄ from many-body methods. *Appl. Phys. Lett.* **98**, 241915.
- Kamoun N, Bouzouita H and Rezig B 2007 Fabrication and characterization of Cu₂ZnSnS₄ thin films deposited by spray pyrolysis technique. *Thin Solid Films* **515**, 5949.
- Katagiri H, Saitoh K, Washio T, Shinohara H, Kurumadani T and Miyajima S 2001 Development of thin film solar cell based on Cu₂ZnSnS₄ thin films. *Sol. Energy Mater. Sol. Cells* **65**, 141.
- Kawazoe H, Yasukawa M, Hyodo H, Kurita M, Yanagi H and Hosono H 1997 P-type electrical conduction in transparent thin films of CuAlO₂. *Nature* **389**, 939.
- Kioupakis E, Zhang P, Cohen ML and Louie SG 2008 GW quasiparticle corrections to the LDA + U/GGA + U electronic structure of bcc hydrogen. *Phys. Rev. B* **77**, 155114.
- Kohn W and Sham LJ 1965 Self-consistent equations including exchange and correlation effects. *Phys. Rev.* **140**, A1133–A1138.
- Kresse G and Furthmüller J 1996a Efficiency of ab-initio total energy calculations for metals and semiconductors using a plane-wave basis set. *Comput. Mater. Sci.* **6**, 15.
- Kresse G and Furthmüller J 1996b Efficient iterative schemes for ab initio total-energy calculations using a plane-wave basis set. *Phys. Rev. B* **54**, 11169–11186.
- Kresse G and Joubert D 1999 From ultrasoft pseudopotentials to the projector augmented-wave method. *Phys. Rev. B* **59**, 1758–1775.
- Lany S and Zunger A 2008 Assessment of correction methods for the band-gap problem and for finite-size effects in supercell defect calculations: Case studies for ZnO and GaAs. *Phys. Rev. B* **78**, 235104.

- Laskowski R, Christensen NE, Blaha P and Palanivel B 2009 Strong excitonic effects in CuAlO₂ delafossite transparent conductive oxides. *Phys. Rev. B* **79**, 165209.
- Łażewski J, Jochym PT and Parlinski K 2002 Band structure, Born effective charges, and lattice dynamics of CuInS from ab initio calculations. *J. Chem. Phys.* **117**, 2726.
- Levchenko S, Syrbu NN, Tezlevan VE, Arushanov E, Doka-Yamigno S, Schedel-Niedrig T and Lux-Steiner MC 2007 Optical spectra and energy band structure of single crystalline CuGaS₂ and CuInS₂. *J. Phys.: Condens. Matter* **19**, 456222.
- Li JL, Rignanese GM, Chang EK, Blase X and Louie SG 2002 GW study of the metal-insulator transition of bcc hydrogen. *Phys. Rev. B* **66**, 035102.
- Marini A, Del Sole R and Rubio A 2003 Bound excitons in time-dependent density-functional theory: Optical and energy-loss spectra. *Phys. Rev. Lett.* **91**, 256402.
- Marini A, Hogan C, Grüning M and Varsano D 2009 yambo: An ab initio tool for excited state calculations. *Comput. Phys. Comm.* **180**, 1392–1403.
- Marques MAL, Vidal J, Oliveira MJT, Reining L and Botti S 2011 Density-based mixing parameter for hybrid functionals. *Phys. Rev. B* **83**, 035119.
- Merino JM *et al.* 1996 Composition effects on the crystal structure of CuInSe. *J. Appl. Phys.* **80**, 5610.
- Mizoguchi H, Hirano M, Fujitsu S, Takeuchi T, Ueda K and Hosono H 2002 ZnRh₂O₄: A p-type semiconducting oxide with a valence band composed of a low spin state of Rh³⁺ in a 4d⁶ configuration. *Appl. Phys. Lett.* **80**, 1207.
- Nagoya A, Asahi R, Wahl R and Kresse G 2010 Defect formation and phase stability of Cu₂ZnSnS₄ photovoltaic material. *Phys. Rev. B* **81**, 113202.
- Nakamura S, Senoh M and Iwasa N 1992 Thermal annealing effects on p-type Mg-doped GaN films. *Jpn. J. Appl. Phys.* **31**, L139.
- Nakayama N and Ito K 1996 Sprayed films of stannite Cu₂ZnSnS₄. *Appl. Surf. Sci.* **92**, 171.
- Neugebauer J and Van de Walle CG 1995 Hydrogen in GaN: Novel aspects of a common impurity. *Phys. Rev. Lett.* **75**, 4452–4455.
- Nie X, Wei S and Zhang S 2002 Bipolar doping and band-gap anomalies in delafossite transparent conductive oxides. *Phys. Rev. Lett.* **88**, 066405.
- Ogo Y, Hiramatsu H, Nomura K, Yanagi H, Kamiya T, Hirano M and Hosono H 2008 p-channel thin-film transistor using p-type oxide semiconductor, SnO. *Appl. Phys. Lett.* **93**, 032113–032113.
- Ohta H, Nomura K, Hiramatsu H, Ueda K, Kamiya T, Hirano M and Hosono H 2003 Frontier of transparent oxide semiconductors. *Solid State Electronics* **47**, 2261–2267.
- Olekseyuk D, Gulay L, Dydchak I, Piskach L, Parasyuk O and Marchuk O 2002 Single crystal preparation and crystal structure of the Cu₂Zn/Cd,Hg/SnSe₄ compounds. *J. Alloys Compd.* **340**, 141.
- Ong C and Gong H 2003 Effects of aluminum on the properties of p-type Cu-Al-O transparent oxide semiconductor prepared by reactive co-sputtering. *Thin Solid Films* **445**, 299–303.
- Onida G, Reining L and Rubio A 2002 Electronic excitations: density-functional versus many-body green's-function approaches. *Rev. Mod. Phys.* **74**, 601–659. and refereces therein.
- Paier J, Asahi R, Nagoya A and Kresse G 2009 Cu₂ZnSnS₄ as a potential photovoltaic material: A hybrid hartree-fock density functional theory study. *Phys. Rev. B* **79**, 115126.
- Paier J, Marsman M and Kresse G 2007. *J. Chem. Phys.* **127**, 024103.
- Paier J, Marsman M and Kresse G 2008 Dielectric properties and excitons for extended systems from hybrid functionals. *Phys. Rev. B* **78**, 121201.
- Partain L, McLeod P, Duisman J, Peterson T, Sawyer D and Dean C 1983 Degradation of a cuxs/cds solar cell in hot, moist air and recovery in hydrogen and air. *J. Appl. Phys.* **54**, 6708–6720.
- Pearson G 1957 Conversion of solar to electrical energy. *American Journal of Physics* **25**, 591.
- Pellicer-Porres J, Segura A and Kim D 2009 Refractive index of the CuAlO₂ delafossite. *Semicond. Sci. Technol.* **24**, 015002.
- Pellicer-Porres J, Segura A, Gilliland A, Munoz A, Rodriguez-Hernandez P, Kim D, Lee M and Kim T 2006 On the band gap of CuAlO₂ delafossite. *Appl. Phys. Lett.* **88**, 181904.
- Perdew JP, Burke K and Ernzerhof M 1996. *Phys. Rev. Lett.* **77**, 3865–8. Erratum: *ibid.* **78**, 1396(E) (1997).
- Persson C 2010 Electronic and optical properties of Cu₂ZnSnS₄ and Cu₂ZnSnSe₄. *J. Appl. Phys.* **107**, 053710.
- Persson C and Zunger A 2005 Compositionally induced valence-band offset at the grain boundary of polycrystalline chalcopyrites creates a hole barrier. *Appl. Phys. Lett.* **87**, 211904.
- Petersilka M, Gossmann UJ and Gross EKV 1996 Excitation energies from time-dependent density-functional theory. *Phys. Rev. Lett.* **76**, 1212–1215.
- Rau U and Schock H 1999 Electronic properties of Cu(In,Ga)Se₂ heterojunction solar cells-recent achievements, current understanding, and future challenges: Thin film solar cells. *Appl. Phys. A* **69**, 131–147.

- Redinger A, Berg DM, Dale PJ and Siebentritt S 2011 The consequences of kesterite equilibria for efficient solar cells. *J. Am. Chem. Soc.* **133**, 3320.
- Reining L, Olevano V, Rubio A and Onida G 2002 Excitonic effects in solids described by time-dependent density-functional theory. *Phys. Rev. Lett.* **88**, 066404.
- Repins I, Contreras MA, Egaas B, DeHart C, Scharf J, Perkins CL, To B and Noufi R 2008 19.9%-efficient ZnO/CdS/CuInGaSe₂ solar cell with 81.2% fill factor. *Prog. Photovolt.* **16**, 235.
- Rife JC, Dexter RN, Bridenbaugh PM and Veal BW 1977 Optical properties of the chalcopyrite semiconductors ZnGeP₂, ZnGeAs₂, CuGaS₂, CuAlS₂, CuInSe₂, and AgInSe₂. *Phys. Rev. B* **16**, 4491–4500.
- Ringeissen J, Regolini JL and Lewonczuk S 1973 Optical properties of CuGaS₂. *Surf. Sci.* **37**, 777–785.
- Rinke P, Qteish A, Neugebauer J, Freysoldt C and Scheffler M 2005 Focus on photoemission and electronic structure combining gw calculations with exact-exchange density-functional theory: an analysis of valence-band photoemission for compound semiconductors. *New J. Phys.* **7**, 126.
- Robertson J, Peacock P, Towler M and Needs R 2002 Electronic structure of p-type conducting transparent oxides. *Thin Solid Films* **411**, 96–100.
- Runge E and Gross EKV 1984 Density-functional theory for time-dependent systems. *Phys. Rev. Lett.* **52**, 997–1000.
- Sasaki M and Shimode M 2003 Fabrication of bipolar CuInO₂ with delafossite structure. *J. Phys. Chem. Solids* **64**, 1675–1679.
- Scanlon D and Watson G n.d. Conductivity limits in CuAlO₂ from screened-hybrid density functional theory. *J. Phys. Chem. Lett.* **1**, 3195–3199.
- Schorr S 2007 Structural aspects of adamantane like multinary chalcogenides. *Thin Solid Films* **515**, 5985.
- Schorr S, Hoebler HJ and Tovar M 2007 A neutron diffraction study of the stannite-kesterite solid solution series. *Eur. J. Mineral.* **19**, 65.
- Seidl A, Görling A, Vogl P, Majewski JA and Levy M 1996 Generalized Kohn-Sham schemes and the band-gap problem. *Phys. Rev. B* **53**, 3764–3774.
- Seol JS, Lee SY, Lee JC, Nam HD and Kim KH 2003 Electrical and optical properties of Cu₂ZnSnS₄ thin films prepared by rf magnetron sputtering process. *Sol. Energy Mater. Sol. Cells* **75**, 155.
- Shah A, Torres P, Tscharnner R, Wyrsh N and Keppner H 1999 Photovoltaic technology: the case for thin-film solar cells. *Science* **285**, 692.
- Sham LJ and Rice TM 1966 Many-particle derivation of the effective-mass equation for the wannier exciton. *Phys. Rev.* **144**, 708–714.
- Sharma S, Dewhurst JK, Sanna A and Gross EKV 2011 Bootstrap approximation for the exchange-correlation kernel of time-dependent density functional theory. *Phys. Rev. Lett.* **107**, 186401.
- Shi L, Fang Z and Li J 2008 First-principles study of p-type transparent conductive oxides CuXO₂ (X = Y, Sc, and Al). *J. Appl. Phys.* **104**, 073527.
- Sottile F, Olevano V and Reining L 2003 Parameter-free calculation of response functions in time-dependent density-functional theory. *Phys. Rev. Lett.* **91**, 056402.
- Stephens P, Devlin FJ, Chabalowski CF and Frisch MJ 1994 Ab initio calculation of vibrational absorption and circular dichroism spectra using density functional force fields. *J. Phys. Chem.* **98**, 11623.
- Strinati G, Mattausch HJ and Hanke W 1982 Dynamical aspects of correlation corrections in a covalent crystal. *Phys. Rev. B* **25**, 2867–2888.
- Stubner R, Tokatly IV and Pankratov O 2004 Excitonic effects in time-dependent density-functional theory: an analytically solvable model. *Phys. Rev. B* **70**, 245119.
- Syrbu NN, Tiginyanu IM, Nemerenco LL, Ursaki VV, Tezlevan VE and Zalamai VV 2005 Exciton spectra, valence band splitting, and energy band structure of CuGa_xIn_{1-x}S₂ and CuGa_xIn_{1-x}Se₂ crystals. *J. Phys. Chem. Solids* **66**, 1974–1977.
- Sze S and Ng K 2007 *Physics of semiconductor devices*. Wiley-Blackwell.
- Tanaka T, Nagatomo T, Kawasaki D, Nishio M, Guo Q, Wakahara A, Yoshida A and Ogawa H 2005. *J. Phys. Chem. Solids* **66**, 1978.
- Tate J, Ju HL, Moon JC, Zakutayev A, Richard AP, Russell J and McIntyre DH 2009 Origin of p-type conduction in single-crystal CuAlO₂. *Phys. Rev. B* **80**, 165206.
- Tell B and Kasper HM 1973 Excitons and the spin-orbit splitting in CuGaS₂. *Phys. Rev. B* **7**, 740–742.
- Teplin CW, Kaydanova T, Young DL, Perkins JD, Ginley DS, Ode A and Readey DW 2004 A simple method for the preparation of transparent p-type Ca-doped CuInO₂ films: Pulsed-laser deposition from air-sintered Ca-doped Cu₂In₂O₅ targets. *Appl. Phys. Lett.* **85**, 3789–3791.
- Thomas G 1997 Materials science: Invisible circuits. *Nature (London)* **389**, 907.
- Todorov K, Reuter KB and D. B. Mitzi 2010 High-efficiency solar cell with earth-abundant liquid-processed absorber. *Adv. Mater.* **22**, E156.

- Trani F, Vidal J, Botti S and Marques MAL 2010 Band structures of delafossite transparent conductive oxides from a self-consistent GW approach. *Phys. Rev. B* **82**, 085115.
- Troullier N and Martins JL 1991 Efficient pseudopotentials for plane-wave calculations. *Phys. Rev. B* **43**, 1993–2006.
- Ueda K, Hase T, Yanagi H, Kawazoe H, Hosono H, Ohta H, Orita M and Hirano M 2001 Epitaxial growth of transparent p-type conducting CuGaO_2 thin films on sapphire (001) substrates by pulsed laser deposition. *J. Appl. Phys.* **89**, 1790–1793.
- Ueda K, Inoue S, Hirose S, Kawazoe H and Hosono H 2000 Transparent p-type semiconductor: LaCuOS layered oxysulfide. *Appl. Phys. Lett.* **77**, 2701.
- van Leeuwen R 2001 Key concepts in time-dependent density-functional theory. *Int. J. Mod. Phys. B* **15**, 1969–2023.
- van Schilfgaarde M, Kotani T and Faleev S 2006 Quasiparticle self-consistent GW theory. *Phys. Rev. Lett.* **96**, 226402.
- Vidal J, Botti S, Olsson P, Guillemoles JF and Reining L 2010a Strong interplay between structure and electronic properties in $\text{CuIn}(\text{S}, \text{Se})_2$: A first-principles study. *Phys. Rev. Lett.* **104**, 056401.
- Vidal J, Trani F, Bruneval F, Marques MAL and Botti S 2010b Effects of electronic and lattice polarization on the band structure of delafossite transparent conductive oxides. *Phys. Rev. Lett.* **104**, 136401.
- von Barth U, Dahlen NE, van Leeuwen R and Stefanucci G 2005 Conserving approximations in time-dependent density functional theory. *Phys. Rev. B* **72**, 235109.
- Wadia C, Alivisatos A and Kammen D 2009 Materials availability expands the opportunity for large-scale photovoltaics deployment. *Environmental science & technology* **43**, 2072.
- Wei SH and Zunger A 1988 Role of metal d states in II-VI semiconductors. *Phys. Rev. B* **37**, 8958–8981.
- Wu X, Keane J, Dhere R, DeHart C, Duda A, Gessert T, Asher S, Levi D and Sheldon P 2001 16.5%-efficient CdS/CdTe polycrystalline thin-film solar cell *Proceedings of the 17th European photovoltaic solar energy conference*, vol. 995 James & James Ltd.: London.
- Xiao HZ, Yang LC and Rockett A 1994 Structural, optical, and electrical properties of epitaxial chalcopyrite CuIn_3Se_5 films. *J. Appl. Phys.* **76**, 1503–1510.
- Yanagi H, Hase T, Ibuki S, Ueda K and Hosono H 2001 Bipolarity in electrical conduction of transparent oxide semiconductor CuInO_2 with delafossite structure. *Appl. Phys. Lett.* **78**, 1583–1585.
- Yanagi H, Inoue S, Ueda K, Kawazoe H, Hosono H and Hamada N 2000 Electronic structure and optoelectronic properties of transparent p-type conducting CuAlO_2 . *J. Appl. Phys.* **88**, 4159–4163.
- Yanagi H, Ueda K, Ohta H, Orita M, Hirano M and Hosono H 2002 Fabrication of all oxide transparent p-n homojunction using bipolar CuInO_2 semiconducting oxide with delafossite structure. *Solid State Comm.* **121**, 15–17.
- Yu RS, Liang SC, Lu CJ, Tasi DC and Shieu FS 2007 Characterization and optoelectronic properties of p-type n-doped CuAlO_2 films. *Appl. Phys. Lett.* **90**, 191117.
- Zakutayev A, Kykyneshi R, Schneider G, McIntyre DH and Tate J 2010 Electronic structure and excitonic absorption in BaCuChF ($\text{Ch}=\text{S}, \text{Se}, \text{and Te}$). *Phys. Rev. B* **81**, 155103.
- Zangwill A and Soven P 1980 Resonant photoemission in barium and cerium. *Phys. Rev. Lett.* **45**, 204–207.
- Zhang J, Shao L, Fu Y and Xie E 2006. *Rare Metals* **25**, 315.
- Zhang SB, Wei S, Zunger A and Katayama-Yoshida H 1998 Defect physics of the CuInSe_2 chalcopyrite semiconductor. *Phys. Rev. B* **57**, 9642.
- Zhao J, Wang A, Green M and Ferrazza F 1998 19.8% efficient honeycomb textured multicrystalline and 24.4% monocrystalline silicon solar cells. *Appl. Phys. Lett.* **73**, 1991.
- Zunger A 2003 Practical doping principles. *Appl. Phys. Lett.* **83**, 57.